



Dynamical analysis of spatio-temporal CoVid-19 model

Mohammad Ghani¹ · Indah Fahmiyah¹ · Ratih Ardiati Ningrum¹ · Ananta Adhi Wardana²

Received: 16 December 2023 / Revised: 29 January 2024 / Accepted: 1 February 2024 / Published online: 25 March 2024
© The Author(s), under exclusive licence to Springer-Verlag GmbH Germany, part of Springer Nature 2024

Abstract

This paper focuses on the spatio-temporal CoVid-19 model. The positivity and boundedness are provided based on the standard positivity theorem. The Picard's iteration is employed to obtain the existence and uniqueness of solution for each state variable. Due to the presence of diffusion terms, the Fourier expansion are employed to provide the locally asymptotical stability for both equilibrium points. Moreover, the appropriate Lyapunov function is a first step before proving the globally asymptotical stability for both equilibrium points. The numerical simulations conclude that the increasing of isolation rate (from $\epsilon = 0.03$ to $\epsilon = 0.9$) is more effective than the decreasing of social distancing rate (from $\delta = 0.4$ to $\delta = 0.04$) in reducing the number of infected individuals, where these results are based on the basic reproduction values, i.e., $\mathcal{R}_0 = 0.8751 < 1$ for change of isolation rate and $\mathcal{R}_0 = 0.9344 < 1$ for change of social distancing rate. The fitting results of our temporal CoVid-19 model with the observed data can be obtained through the least-square technique, neural network, and extended Kalman filter. Based on the model parameters, then we employ neural network (NN) consisting of Levenberg–Marquadt as the training function and Tangent Sigmoid and Purelin as two activation functions to fit the temporal model. The fitting results using neural network of SIQR model are significant based on the mean squared error. Due to the significant results of fitting using extended Kalman filter, we also provide this technique by choosing two tuning parameters of $Q = \text{diag}([10 \ 10 \ 10 \ 5])$ and $R = \text{diag}([100 \ 10 \ 10 \ 1])$ for the covariance of process and observation respectively. Moreover, we have the smallest RMSE and MSE of EKF in the date range of \mathcal{D}_1 with the computation time 13.002942 s and the fastest computation of EKF in the date range of \mathcal{D}_5 with the RMSE 0.014 and the MSE 1.9550e–04. The smallest RMSE and MSE of NN are shown in the date range of \mathcal{D}_1 with the computation time 11.442112 in unit of seconds and the fastest computation of NN is provided in the date range of \mathcal{D}_2 with the RMSE 0.0253 and MSE 6.4100e–04.

Keywords Spatio-temporal model · CoVid-19 · Transmission rate · Least-square technique · Neural network · Extended Kalman filter (EKF)

Mathematics Subject Classification 35A01 · 35B40

1 Introduction

The form of Covid-19 was caused by a Coronavirus endemic since 2019. Fever and shortness of breath are among the symptoms of Coronaviruses. Indonesia experienced the first outbreak of Covid-19 on March 2, 2020 [1]. As of yet,

there has been no end to the Covid-19 epidemic. Using data accessed through covid.19.go.id, 14,657 active covid-19 cases are recorded in Indonesia. To avoid an increase in Covid-19 cases, the Ministry of Health has urged people to wear masks again. In Indonesia, a new Covid-19 variant, the Arcturus variant, has entered the market, causing an increase in Covid-19. This variant disease leads to fever, coughing, muscle aches, and conjunctivitis. A variant of Arcturus was first time discovered in India in January 2023. Arcturus was formed as a result of homologous recombination between two or more sub-lineages [2]. According to the Health Ministry of Indonesia, in mid-April 2023, the cases number of the Arcturus variant significantly increased. By applying mathematics to disease outbreaks, it is possible to predict their

✉ Mohammad Ghani
mohammad.ghani2013@gmail.com

¹ Data Science Technology, Faculty of Advanced Technology and Multidiscipline, Universitas Airlangga, Surabaya 60115, Indonesia

² Robotics Engineering and Artificial Intelligence, Faculty of Advanced Technology and Multidiscipline, Universitas Airlangga, Surabaya 60115, Indonesia

spread. Using a simple mathematical model, SI (Susceptible-Infection) is applied to the spread of Covid-19. By utilizing the Bernoulli Verhulst model, the SI model can derive identification parameters [3]. When Covid-19 spreads throughout the population, the SIR model can be used to predict how many will need medical treatment [4]. An appropriate Lyapunov function and LaSalle invariant technique were applied to the SIR model of Covid-19 to reduce the spread of Covid-19 based on room availability [5]. We examine Covid-19's transmission by applying the classic Kermack–McKendrick model. Malaysia's first wave of Covid-19 infection was also examined with the SIR model. It has been shown that cleanliness awareness and social distancing can help to reduce Covid-19 transmission in this study [6]. The Covid-19's transmission through SIR model in an area can be implemented a control when local restrictions are implemented and strong policies are in [7]. It is determined that the SIR model relies on the parameters of interaction level and intensity of recovery [8]. A numerical solution of SIR model was obtained with the convex event rate by using the nonstandard finite difference method [9]. The SIR spread model is found to be more useful in a short-term comparison with the Verhulst, Gompertz and SIR spread models [10]. The Covid-19 spreads through SIR model under the influence of the health system were locally stable if the basic reproduction number becomes less than one [11].

A short-term and long-term prediction of Covid-19's spread through the *SIRD* model was studied in [12]. Using the *SIRD* model, short-term infection with Covid-19 can be predicted [13]. Indonesia implemented a *SIRD* model to provide the estimation of Covid-19's transmission for the long-term prediction [14]. By considering the sex and age filters, the *SIRD* model predicts that a younger population gets much more possible than an older population to become infected with Covid-19 [15]. Countless countries can be affected by Covid-19, as the *SIRD* model estimates that its basic reproduction number more than one. There are exposed individuals of CoVid-19, which are not necessarily positive test yet still in symptom conditions. Moreover, the exposed subpopulation of the SEIR model demonstrates the importance of controlling Covid-19's impact [16]. According to the SEIR model, the increase of recovered population was reported in Indonesia after vaccination and isolation for the Covid-19 case [17]. In the case of Covid-19, the *A – SIRV* model employs variational imbedding to estimate the spread of the outbreak [18]. It takes more than one vaccination to protect against COVID-19. Sepulveda et al. studied the mathematical models by introducing the first and second immunizations. The behavior of Covid-19 following the first vaccination is described in the study [19]. The mathematical model known as *SVIR* (susceptible-vaccine-infection-removed) makes the assumption that susceptible people will receive vaccinations. The *SVIR* model's ordi-

nary least squares are used in this investigation [20]. The benefits of Indonesia's vaccination program may be increased by allocating vaccines according to the Covid-19 outbreak that is spreading the fastest [21]. Eventhough the vaccinations have been implemented, but the Covid-19 disease can reinfect the susceptible individuals. The quarantine for the exposed individuals of Covid-19 is a method to take care of its transmission. A SIQR model can be used to study the spread of Covid-19 disease consisting of susceptible, infected, quarantined and recovered individuals [22]. The SIQR model is appropriate for locations that implement the quarantine restrictions in place. Based on the studies of the SIQR model, significant loudness leads to the disease vanished exponentially, establishing the necessary circumstances for the existence of a unique stationary distribution [23]. The fractional derivative of Atangana–Beleanu–Caputo was used to provide SIQR model for the spread of Covid-19 [24]. This study demonstrates that quarantine can degrade the transmission rate of Covid-19. The positivity and convergence are achieved while approaching towards the stability by using the nonstandard finite difference (NSFD)[25]. By using the fractional model, disease control decisions can be made more flexible than with a classical derivative [26]. Fractional models can be used to observe unpredictable dynamic behavior and control noise. The Covid-19 disease spread model based on the government intervention and public perception produced better results than the integer order model [27]. Based on a fractional model incorporating symptomatic and asymptomatic effects, it can be shown that recruitment rate and symptomatic transmission influence reproduction [28]. The Covid-19 Fractional Model shows that vaccination can reduce deaths [29]. With the presence of the novel Arcurus Covid-19 strain into Indonesia, preventive measures such as quarantine are required. Researchers are interested in how Covid-19 spreads can be handled by the control implementation of social distancing, studying the locally and globally stability of disease-free and endemic. Moreover, the study of data-driven CoVid-19 model with comorbidity was investigated in [30] and the CoVid-19 model with comorbidity and implementation of control using non-pharmaceutical interventions and vaccination was studied in [31].

2 Model formulation

The dynamical system of CoVid-19 disease consisting of the susceptible individuals (S), infected individuals (I), quarantined individuals (Q) and recovered individuals (R) is provided in this section. We first consider the following CoVid-19 model with social distancing (δ) and isolation rate (ϵ):

$$\begin{aligned}\frac{dS}{dt} &= \Lambda - \beta\delta SI - \mu S, \\ \frac{dI}{dt} &= \beta\delta SI - (r + \epsilon + \mu + d)I, \\ \frac{dQ}{dt} &= \epsilon I - (\varphi + d + \mu)Q, \\ \frac{dR}{dt} &= rI + \varphi Q - \mu R,\end{aligned}\tag{2.1}$$

where the birth rate, the transmission rate, the social distancing, the natural death rate, the cure rate related to infected, the isolation rate, the death rate related to disease and the cure rate related to isolation are mathematically expressed as Λ , β , δ , μ , r , ϵ , d and φ respectively. Moreover, the CoVid-19 spread is consider not only in time but also in space. Due to this reason, then Eq. (2.1) becomes

$$\begin{aligned}\frac{\partial S}{\partial t} &= D_1 \Delta S + \Lambda - \beta\delta SI - \mu S, \\ \frac{\partial I}{\partial t} &= D_2 \Delta I + \beta\delta SI - (r + \epsilon + \mu + d)I, \\ \frac{\partial Q}{\partial t} &= D_3 \Delta Q + \epsilon I - (\varphi + d + \mu)Q, \\ \frac{\partial R}{\partial t} &= D_4 \Delta R + rI + \varphi Q - \mu R,\end{aligned}\tag{2.2}$$

for $(x, t) \in \Omega \times (0, +\infty)$, the initial conditions,

$$\begin{aligned}S(x, 0) &= S_0, \quad I(x, 0) = I_0, \quad Q(x, 0) = Q_0, \\ R(x, 0) &= R_0, \quad x \in \bar{\Omega},\end{aligned}\tag{2.3}$$

and the homogeneous Neumann boundary conditions

$$\begin{aligned}\frac{\partial S(x, t)}{\partial \phi} &= \frac{\partial I(x, t)}{\partial \phi} = \frac{\partial Q(x, t)}{\partial \phi} \\ &= \frac{\partial R(x, t)}{\partial \phi} = 0, \quad (x, t) \in \partial\Omega \times (0, +\infty),\end{aligned}\tag{2.4}$$

where ϕ is the outward unit normal vector on the boundary.

Remark 1 This paper is a modified version of the study in [32, 33], in which the rate of social distancing and isolation is introduced. According to the findings, the social distancing (δ) and isolation rate (ϵ) can effectively degrade the transmission rate of CoVid-19, where no social distancing occurs if δ equals to one and full social distancing occurs if δ equals to zero. Moreover, we consider that CoVid-19 can be transmitted over time and space.

2.1 Equilibrium points

Theorem 2.1 Let the parameters be positive. Then one has the disease-free equilibrium point $\mathcal{E}_0 = \left(\frac{\Lambda}{\mu}, 0, 0, 0\right)$ if $\mathcal{R}_0 <$

1 and $\mathcal{E}_1 = \left(\frac{r+\epsilon+\mu+d}{\beta\delta}, \frac{\Lambda}{r+\epsilon+\mu+d} - \frac{\mu}{\beta\delta}, \frac{\epsilon I^*}{\varphi+d+\mu}, \frac{rI^*}{\mu} + \frac{\varphi Q^*}{\mu}\right)$ as the endemic equilibrium point if $\mathcal{R}_0 > 1$. Moreover, the basic reproduction number is given as $\mathcal{R}_0 = \frac{\Lambda\beta\delta}{\mu(r+\epsilon+\mu+d)}$.

Proof We first consider the steady-states $\frac{dS}{dt} = \frac{dI}{dt} = \frac{dQ}{dt} = \frac{dR}{dt} = 0$ in the Eq. (2.1), then one can derive

$$\begin{aligned}0 &= \Lambda - \beta\delta SI - \mu S, \\ 0 &= \beta\delta SI - (r + \epsilon + \mu + d)I, \\ 0 &= \epsilon I - (\varphi + d + \mu)Q, \\ 0 &= rI + \varphi Q - \mu R.\end{aligned}\tag{2.5}$$

At the disease-free, we assume that $I = Q = R = 0$ in Eq. (2.5). Otherwise, it is called as endemic assumptions. Then, one has the following two equilibrium points for disease-free and endemic respectively

$$\mathcal{E}_0 = (S^0, I^0, Q^0, R^0) = \left(\frac{\Lambda}{\mu}, 0, 0, 0\right),\tag{2.6}$$

and

$$\mathcal{E}_1 = (S^*, I^*, Q^*, R^*),\tag{2.7}$$

where

$$\begin{aligned}S^* &= \frac{r + \epsilon + \mu + d}{\beta\delta}, \quad I^* = \frac{\Lambda}{r + \epsilon + \mu + d} - \frac{\mu}{\beta\delta}, \\ Q^* &= \frac{\epsilon}{\varphi + d + \mu} I^*, \quad R^* = \frac{r}{\mu} I^* + \frac{\varphi}{\mu} Q^*.\end{aligned}$$

As the first step of determining the basic reproduction number. We apply the linearization at equilibrium point \mathcal{E}_0 , then we obtain two matrices of \mathcal{M} and \mathcal{P} which are respectively as the new infected individuals transmission and individual displacements transition for both two individual groups as shown as follows

$$\begin{aligned}\mathcal{M} &= \begin{pmatrix} \beta\delta S & 0 \\ 0 & 0 \end{pmatrix} \\ \mathcal{P} &= \begin{pmatrix} r + \epsilon + \mu + d & 0 \\ -\epsilon & \varphi + d + \mu \end{pmatrix}.\end{aligned}$$

Moreover, the next generation matrix is given below

$$\mathcal{MP}^{-1} = \begin{pmatrix} \frac{\Lambda\beta\delta}{\mu(r+\epsilon+\mu+d)} & 0 \\ 0 & 0 \end{pmatrix}$$

Based on the next generation matrix, one can determine the dominant eigenvalues. Hence, the basic reproduction number are expressed as follows

$$\mathcal{R}_0 = \frac{\Lambda\beta\delta}{\mu(r + \epsilon + \mu + d)}.\tag{2.8}$$

□

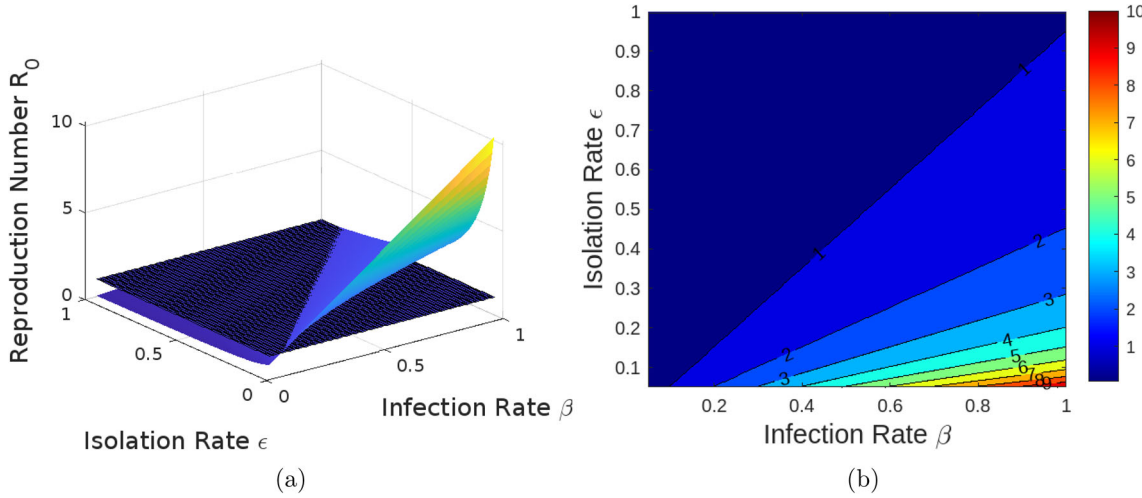


Fig. 1 Dependency of R_0 on infection rate β and isolation rate ϵ

Figure 1 represents the dependency of basic reproduction number R_0 on infection rate β and isolation rate ϵ . As the reproduction number R_0 increases then the infection rate β also increases. Otherwise, as the reproduction number R_0 decreases but the isolation rate ϵ increases. Then, the strategy of increasing the isolation rate can decrease the viruses spread and this strategy is also the most effective to provide the reproduction number R_0 less than 1.

2.2 Positivity and Boundedness

We first provide the following standard positivity theorem.

Theorem 2.2 Let $\mathcal{Z} \in [C(\bar{\Omega} \times [0, \tau)) \cap C^{2,1}(\Omega \times (0, \tau))]$ and satisfies

$$\begin{aligned} \mathcal{Z}_t - D\Delta\mathcal{Z} &\geq \mathcal{U}(x, t)\mathcal{Z}, \quad x \in \Omega, \quad 0 < t \leq \tau, \\ \frac{\partial \mathcal{Z}}{\partial n} &\geq 0, \quad x \in \partial\Omega, \quad 0 < t \leq \tau, \\ \mathcal{Z}(x, 0) &\geq 0, \quad x \in \bar{\Omega}, \end{aligned}$$

where $\mathcal{U} \in C(\bar{\Omega} \times [0, \tau])$. Then, $\mathcal{Z}(x, t) \geq 0$ on $\bar{\Omega} \times [0, \tau]$ and $\mathcal{Z} > 0$ or $\mathcal{Z} \equiv 0$ in $\bar{\Omega} \times (0, \tau]$.

Theorem 2.2 is consequence of the following positivity of dynamical system (2.2).

Theorem 2.3 Let $S(x, t)$, $I(x, t)$, $Q(x, t)$ and $R(x, t)$ be the solution of (2.2) with the initial conditions (2.3). Then, for $(x, t) \in \Omega \times (0, +\infty)$, $S(x, t)$, $I(x, t)$, $Q(x, t)$ and $R(x, t)$ are positive.

Proof For any τ with $0 < \tau \leq T$, where T is the maximal existing time. By applying Theorem 2.2 directly, then one has $S(x, t) > 0$ in $\Omega \times (0, \tau]$. We further have $(I, Q)(x, t) > 0$,

because of the following two conditions

$$\begin{aligned} \frac{\partial I}{\partial t} - D_2\Delta I &\geq -(r + \epsilon + \mu + d)I, \\ \frac{\partial Q}{\partial t} - D_3\Delta Q &\geq -(\varphi + d + \mu)Q, \end{aligned}$$

for $(x, t) \in \Omega \times (0, \tau]$. We further investigate that $R(x, t) > 0$ in $\Omega \times (0, \tau]$. Otherwise, one can find $x^* \in \Omega$ such that $R(x^*, t^*) = 0$ and $R(x^*, t) > 0$ in $\bar{\Omega} \times (0, t^*)$, for $t^* \leq \tau$, i.e., (x^*, t^*) is the minimum point of the function $R(x, t)$ in $\bar{\Omega} \times (0, t^*]$. Then, one can derive

$$\begin{aligned} \frac{\partial R}{\partial t} - D_4\Delta R &\leq 0, \\ rI + \varphi Q - \mu R &\geq rI > 0, \end{aligned}$$

at the point (x^*, t^*) , which is contradict with the fourth equation of (2.2). Therefore, $R(x, t) > 0$. \square

Theorem 2.4 Suppose $(S, I, Q, R)(x, t) \in [C(\bar{\Omega} \times [0, T)) \cap C^{2,1}(\Omega \times (0, T))]^4$ be the solution of (2.2) with the initial conditions (2.3). Then, for $(x, t) \in \Omega \times (0, +\infty)$, $S(x, t)$, $I(x, t)$, $Q(x, t)$ and $R(x, t)$ are bounded that

$$\begin{aligned} 0 < (S + I + Q + R)(x, t) \\ &\leq \max \left\{ \|S_0 + I_0 + Q_0 + R_0\|_\infty, \frac{\Lambda}{\mu} \right\}. \end{aligned}$$

Proof We first assume that $\mathcal{N}(x, t) = (S + I + Q + R)(x, t)$ is the total population. Differentiating it with respect to t , then we obtain

$$\begin{aligned} \frac{\partial \mathcal{N}(x, t)}{\partial t} &= \frac{\partial S(x, t)}{\partial t} + \frac{\partial I(x, t)}{\partial t} + \frac{\partial Q(x, t)}{\partial t} + \frac{\partial R(x, t)}{\partial t} \\ &= (D_1 + D_2 + D_3 + D_4)\Delta\mathcal{N} + \Lambda \\ &\quad - \mu\mathcal{N}(x, t) - d(I + Q). \end{aligned}$$

Note that

$$\begin{aligned} 0 < \mathcal{N}(t) &\leq \|\mathcal{N}_0\|_\infty \text{ and } \frac{\partial \mathcal{N}(x, t)}{\partial t} \\ &\quad - (D_1 + D_2 + D_3 + D_4)\Delta \mathcal{N} \\ &\leq \Lambda - \mu \mathcal{N}(x, t). \end{aligned}$$

Then, one can derive

$$0 < \mathcal{N}(x, t) \leq \mathcal{U}(t),$$

where

$$\begin{aligned} \mathcal{U}(t) &= \left(\frac{\Lambda}{\mu} + \left(\|\mathcal{N}_0\|_\infty - \frac{\Lambda}{\mu} \right) \exp(-\Lambda t) \right) \\ &\text{for } t \in [0, +\infty) \end{aligned}$$

is the solution of the problem

$$\frac{d\mathcal{U}}{dt} = \Lambda - \mu \mathcal{U}, \quad \mathcal{U}(0) = \|\mathcal{N}_0\|_\infty.$$

Hence, we can derive

$$0 < \mathcal{U}(t) \leq \max \left\{ \|\mathcal{N}_0\|_\infty, \frac{\Lambda}{\mu} \right\}.$$

Therefore, one finally gets

$$0 < \mathcal{N}(x, t) \leq \mathcal{U}(t) \leq \max \left\{ \|\mathcal{N}_0\|_\infty, \frac{\Lambda}{\mu} \right\}.$$

Due to $\mathcal{N}(x, t) = (S + I + Q + R)(x, t)$, the proof is completed. \square

2.3 Existence and Uniqueness

Theorem 2.5 Let $p > 1$, $T > 0$ and the function $\mathcal{F} : [0, T] \times \mathbb{R} \rightarrow \mathbb{R}$ satisfies

$$\begin{aligned} \sup_{x \in \mathbb{R}} |\mathcal{F}(x, t)| &\leq \beta_1(t), \quad \sup_{x, y \in \mathbb{R}, x \neq y} \left| \frac{\mathcal{F}(x, t) - \mathcal{F}(y, t)}{x - y} \right| \\ &\leq \beta_2(t). \end{aligned}$$

for some $(\beta_1, \beta_2)(t) \in L^1(0, T) \times L^p(0, T)$ and $t \in [0, T]$. Thus, for any $y_0 \in \mathbb{R}$ one has $Y : [0, T] \rightarrow \mathbb{R}$ which is unique continuous and satisfies

$$\begin{aligned} \dot{Y}(t) &= \mathcal{F}(t, Y(t)) \text{ for almost everywhere } t \in [0, T], \\ Y(0) &= y_0. \end{aligned} \tag{2.9}$$

Proof We can express Eq. (2.9) as

$$Y(t) = y_0 + \int_0^t \mathcal{F}(\tau, Y(\tau)) d\tau \quad t \in [0, T]. \tag{2.10}$$

Employing the Picard's iteration to Eq. (2.10), one can derive

$$\begin{aligned} Y_{n+1}(t) &= y_0 + \int_0^t \mathcal{F}(\tau, Y_n(\tau)) d\tau \quad t \in [0, T], \\ Y_0(t) &= y_0. \end{aligned} \tag{2.11}$$

Moreover, $Y_n : [0, T] \rightarrow \mathbb{R}$ is continuous and for each n it satisfies

$$\begin{aligned} \|Y_n - Y_0\|_{L^\infty(0, T)} &\leq \int_0^T \sup_{Y_{n-1} \in \mathbb{R}} |\mathcal{F}(\tau, Y_n(\tau))| d\tau \\ &\leq \int_0^T \beta_1(\tau) d\tau = \|\beta_1\|_{L^1(0, T)}. \\ \|Y_{n+1} - Y_n\|_{L^\infty(0, T)} &\leq \int_0^T \sup_{(Y_n, Y_{n-1}) \in \mathbb{R}, Y_n \neq Y_{n-1}} |\mathcal{F}(\tau, Y_n(\tau)) - \mathcal{F}(\tau, Y_{n-1}(\tau))| d\tau \\ &\leq \sup_{(Y_n, Y_{n-1}) \in \mathbb{R}, Y_n \neq Y_{n-1}} \left| \int_0^T (Y_n(t) - Y_{n-1}(t)) d\tau \right| \\ &\int_0^T \beta_2(\tau) d\tau \\ &\leq \sup_{(Y_n, Y_{n-1}) \in \mathbb{R}, Y_n \neq Y_{n-1}} \left| \int_0^T (Y_n(t) - Y_{n-1}(t)) d\tau \right| \\ &\int_0^T (\beta_2(\tau)^p)^{\frac{1}{p}} (t_*)^{1-\frac{1}{p}} d\tau \leq \frac{1}{2} \|Y_n - Y_{n-1}\|_{L^\infty(0, T)}. \end{aligned}$$

where $\|\beta_2\|_{L^p(0, T)} t_*^{1-\frac{1}{p}} \leq \frac{1}{2}$ for any $n \geq 1$ has been employed and $t_* \leq T$. Repeating the process, one has

$$\begin{aligned} \|Y_{n+1} - Y_n\|_{L^\infty(0, T)} &\leq \frac{1}{2} \|Y_n - Y_{n-1}\| \\ &\leq \frac{1}{2^2} \|Y_{n-1} - Y_{n-2}\|_{L^\infty(0, T)} \dots \leq \frac{1}{2^n} \|\beta_1\|_{L^1(0, T)}. \end{aligned}$$

which completes the proof of existence. Moreover, we assume that $m(t) = (n_1 - n_2)(t)$ to provide the proof of uniqueness. Similarly, one has

$$\begin{aligned} \|m\|_{L^\infty(0, T)} &\leq \int_0^T \sup_{(n_1, n_2) \in \mathbb{R}, n_1 \neq n_2} |n_1(\tau) - n_2(\tau)| d\tau \\ &\int_0^T \beta_2(\tau) d\tau \\ &\leq \|m\|_{L^\infty(0, T)} \int_0^T (\beta_2(\tau)^p)^{\frac{1}{p}} (t_*)^{1-\frac{1}{p}} d\tau \\ &\leq \frac{1}{2} \|m\|_{L^\infty(0, T)}. \end{aligned}$$

Hence, $\|m\|_{L^\infty(0, T)} = 0$ is the only one solution satisfying the above inequality. Therefore, the uniqueness is satisfied. \square

2.4 Stability

Theorem 2.6 Let $\mathcal{R}_0 < 1$. Then, the locally asymptotical stability of equilibrium point \mathcal{E}_0 exists.

Proof We first define the following Fourier expansion formula

$$\begin{aligned} S(x, t) &= \sum_k S_k e^{\zeta t} \sin(kx), \\ I(x, t) &= \sum_k I_k e^{\zeta t} \sin(kx), \\ Q(x, t) &= \sum_k Q_k e^{\zeta t} \sin(kx), \\ R(x, t) &= \sum_k R_k e^{\zeta t} \sin(kx). \end{aligned} \quad (2.12)$$

Then, we substitute Eq. (2.12) into (2.2) to get

$$\begin{aligned} \sum_k (\mathcal{W}_{11} - D_1 k^2 - \zeta) S_k + \sum_k \mathcal{W}_{12} I_k \\ + \sum_k \mathcal{W}_{13} Q_k + \sum_k \mathcal{W}_{14} R_k = 0, \\ \sum_k \mathcal{W}_{21} S_k + \sum_k (\mathcal{W}_{22} - D_2 k^2 - \zeta) Q_k \\ + \sum_k \mathcal{W}_{23} I_k + \sum_k \mathcal{W}_{24} R_k = 0, \\ \sum_k \mathcal{W}_{31} S_k + \sum_k \mathcal{W}_{32} I_k \\ + \sum_k (\mathcal{W}_{33} - D_3 k^2 - \zeta) R_k + \sum_k \mathcal{W}_{34} Q_k = 0, \\ \sum_k \mathcal{W}_{41} S_k + \sum_k \mathcal{W}_{42} I_k \\ + \sum_k \mathcal{W}_{43} Q_k + \sum_k (\mathcal{W}_{44} - D_4 k^2 - \zeta) R_k = 0. \end{aligned} \quad (2.13)$$

According to (2.13), the Jacobian matrix can be expressed as follows

$$J = \begin{pmatrix} \mathcal{W}_{11} - D_1 k^2 - \zeta & \mathcal{W}_{12} & \mathcal{W}_{13} & \mathcal{W}_{14} \\ \mathcal{W}_{21} & \mathcal{W}_{22} - D_2 k^2 - \zeta & \mathcal{W}_{23} & \mathcal{W}_{24} \\ \mathcal{W}_{31} & \mathcal{W}_{32} & \mathcal{W}_{33} - D_3 k^2 - \zeta & \mathcal{W}_{34} \\ \mathcal{W}_{41} & \mathcal{W}_{42} & \mathcal{W}_{43} & \mathcal{W}_{44} - D_4 k^2 - \zeta \end{pmatrix}, \quad (2.14)$$

where

$$\begin{aligned} \mathcal{W}_{11} &= -(\beta\delta I + \mu), \quad \mathcal{W}_{12} = -\beta\delta S, \quad \mathcal{W}_{13} = 0, \quad \mathcal{W}_{14} = 0, \\ \mathcal{W}_{21} &= \beta\delta I, \quad \mathcal{W}_{22} = \beta\delta S - (r + \epsilon + \mu + d), \\ \mathcal{W}_{23} &= 0, \quad \mathcal{W}_{24} = 0, \\ \mathcal{W}_{31} &= 0, \quad \mathcal{W}_{32} = \epsilon, \quad \mathcal{W}_{33} = -(\varphi + d + \mu), \quad \mathcal{W}_{34} = 0, \\ \mathcal{W}_{41} &= 0, \quad \mathcal{W}_{42} = r, \quad \mathcal{W}_{43} = \varphi, \quad \mathcal{W}_{44} = -\mu. \end{aligned}$$

Applying the equilibrium point \mathcal{E}_0 to (2.14), we obtain

$$\begin{aligned} J(\mathcal{E}_0) &= \begin{pmatrix} \mathcal{A}_0 - \frac{\Lambda\beta\delta}{\mu} & 0 & 0 \\ 0 & \mathcal{B}_0 & 0 \\ 0 & \epsilon & \mathcal{C}_0 \\ 0 & r & \varphi \end{pmatrix}, \\ \mathcal{A}_0 &= -(\mu + D_1 k^2 + \zeta), \quad \mathcal{B}_0 = \frac{\Lambda\beta\delta}{\mu} \\ &\quad - (r + \epsilon + \mu + d) - (D_2 k^2 + \zeta), \\ \mathcal{C}_0 &= -(\varphi + d + \mu + D_3 k^2 + \phi), \quad \mathcal{D}_0 = -(\mu + D_4 k^2 + \zeta). \end{aligned} \quad (2.15)$$

From the formula $|J(\mathcal{E}_0) - \lambda I_d| = 0$ and Eq. (2.15), one can determine the characteristic equation as follows

$$\begin{aligned} &(-(\mu + D_4 k^2 + \zeta) - \lambda)(-(\varphi + d + \mu + D_3 k^2 + \zeta) - \lambda) \\ &\quad (-(\mu + D_1 k^2 + \zeta) - \lambda) \\ &\quad \left(\frac{\Lambda\beta\delta}{\mu} - (r + \epsilon + \mu + d + D_2 k^2 + \zeta) - \lambda \right) = 0. \end{aligned} \quad (2.16)$$

From (2.16), one can find the eigenvalues $\lambda_1 = -(\mu + D_4 k^2 + \zeta) < 0$, $\lambda_2 = -(\varphi + d + \mu + D_3 k^2 + \zeta) < 0$, $\lambda_3 = -(\mu + D_1 k^2 + \zeta) < 0$ and $\lambda_4 = (r + \epsilon + \mu + d)(\mathcal{R}_0 - 1) - (D_2 k^2 + \zeta)$. Then, we can conclude that $\lambda_4 < 0$ only if $\mathcal{R}_0 < 1$. \square

Theorem 2.7 Let $\mathcal{R}_0 > 1$. Then, the locally asymptotical stability of equilibrium point \mathcal{E}_1 exists.

Proof Similarly. One can determine the following Jacobian matrix at the equilibrium point \mathcal{E}_1

$$J(\mathcal{E}_1) = \begin{pmatrix} \mathcal{A}_* & -\beta\delta S^* & 0 & 0 \\ \beta\delta I^* & \mathcal{B}_* & 0 & 0 \\ 0 & \epsilon & \mathcal{C}_* & 0 \\ 0 & r & \varphi & \mathcal{D}_* \end{pmatrix}, \quad (2.17)$$

where

$$\begin{aligned}\mathcal{A}_* &= -(\beta\delta I^* + \mu + D_1 k^2 + \zeta), \\ \mathcal{B}_* &= \beta\delta S^* - (r + \epsilon + \mu + d + D_2 k^2 + \zeta), \\ \mathcal{C}_* &= -(\varphi + d + \mu + D_3 k^2 + \zeta), \quad \mathcal{D}_* = -(\mu + D_4 k^2 + \zeta).\end{aligned}$$

From the formula $|J(\mathcal{E}_1) - \lambda I_d| = 0$ and Eq. (2.17), one can find the eigenvalues from the characteristic equations

$$\begin{aligned}\lambda_1 &= -(\mu + D_4 k^2 + \zeta) < 0, \\ \lambda_2 &= -(\varphi + d + \mu + D_3 k^2 + \zeta) < 0.\end{aligned}$$

It follows from the Routh–Hurwitz criterion, the following two conditions are given to ensure that the eigenvalues $\lambda_{3,4}$ will be real and negative

$$\lambda_3 + \lambda_4 < 0, \quad \lambda_3 \cdot \lambda_4 > 0.$$

Therefore, one can derive

$$\begin{aligned}\lambda_3 + \lambda_4 &= -\left(\frac{\Lambda\beta\delta}{r + \epsilon + \mu + d} + 2\zeta + (D_1 + D_2)k^2\right) < 0, \\ \lambda_2 \cdot \lambda_3 &= \left(\frac{\Lambda\beta\delta}{r + \epsilon + \mu + d} + D_1 k^2 + \zeta\right)(D_2 k^2 + \zeta) \\ &\quad + \mu(\mathcal{R}_0 - 1)(r + \epsilon + \mu + d).\end{aligned}$$

Hence, $\lambda_3 \cdot \lambda_4 > 0$ if $\mathcal{R}_0 > 1$. Since the Routh–Hurwitz criterion is satisfied for the polynomial $p(\lambda) = \lambda^2 + a_1\lambda + a_2$, i.e., $a_1 > 0$ and $a_1 \cdot a_2 > 0$. Finally, one can find all eigenvalues satisfying Theorem 2.7. \square

Theorem 2.8 Let $\mathcal{R}_0 < 1$. Then, the globally asymptotical stability of equilibrium point \mathcal{E}_0 exists.

Proof The Lyapunov function is first given below

$$L_{\mathcal{E}_0}(t) = \int_{\Omega} \left[\frac{S^2(x, t)}{2} - S^0 S(x, t) + \frac{I^2(x, t)}{2} \right] dx.$$

Differentiating it with respect to t and then one can provide

$$\begin{aligned}\frac{dL_{\mathcal{E}_0}(t)}{dt} &= \int_{\Omega} \left[(S(x, t) - S^0) \frac{\partial S(x, t)}{\partial t} + I(x, t) \frac{\partial I(x, t)}{\partial t} \right] dx \\ &= \int_{\Omega} \left[(S(x, t) - S^0)(D_1 \Delta S(x, t) \right. \\ &\quad \left. + \Lambda - \beta\delta S(x, t)I(x, t) - \mu S(x, t)\right] dx \\ &\quad + \int_{\Omega} [D_2 I(x, t) \Delta I(x, t) + \beta\delta S(x, t)I^2(x, t) \\ &\quad - (r + \epsilon + \mu + d)I^2(x, t)] dx.\end{aligned}\tag{2.18}$$

Substituting the equilibrium points into (2.18), one gets

$$\begin{aligned}\frac{dL_{\mathcal{E}_0}(t)}{dt} &\leq \int_{\Omega} \left[(S(x, t) - S^0)(D_1 \Delta S(x, t) \right. \\ &\quad \left. + \mu S^0 - \mu S(x, t)) \right] dx \\ &\quad + \int_{\Omega} \left[D_2 I(x, t) \Delta I(x, t) + \frac{\Lambda\beta\delta}{\mu} I^2(x, t) \right. \\ &\quad \left. - (r + \epsilon + \mu + d)I^2(x, t) \right] dx.\end{aligned}\tag{2.19}$$

We see that the implementation of the divergence theorem together with the boundary conditions (2.4) can give

$$\begin{aligned}0 &= \int_{\partial\Omega} S^0 \nabla S(x, t) \cdot \phi \, dx \\ &= \int_{\Omega} \operatorname{div} (S^0 \nabla U(x, t)) \, dx \\ &= \int_{\Omega} S^0 \Delta S(x, t), \\ 0 &= \int_{\partial\Omega} S(x, t) \nabla S(x, t) \cdot \phi \, dx \\ &= \int_{\Omega} \operatorname{div} (S(x, t) \nabla S(x, t)) \, dx \\ &= \int_{\Omega} (S(x, t) \Delta S(x, t) + |\nabla S(x, t)|^2),\end{aligned}\tag{2.20}$$

and

$$\begin{aligned}\int_{\Omega} \Delta S(x, t) \, dx &= \int_{\partial\Omega} \frac{\partial S(x, t)}{\partial \phi} \, dx = 0, \\ \int_{\Omega} \Delta I(x, t) \, dx &= \int_{\partial\Omega} \frac{\partial I(x, t)}{\partial \phi} \, dx = 0.\end{aligned}\tag{2.21}$$

Substituting Eqs. (2.20) and (2.21) into Eq. (2.19), we obtain

$$\begin{aligned}\frac{dL_{\mathcal{E}_0}(t)}{dt} &\leq -\mu \int_{\Omega} (S - S^0)^2 \, dx - \int_{\Omega} (1 - \mathcal{R}_0) |I^2(x, t)| \, dx \\ &\quad - D_1 \int_{\Omega} |\nabla S(x, t)|^2 \, dx - D_2 \int_{\Omega} |\nabla I(x, t)|^2 \, dx \\ &\leq -\mathcal{M} \int_{\Omega} ((S(x, t) - S^0)^2 + (I(x, t) - 0)^2 \\ &\quad + |\nabla S(x, t)|^2 + |\nabla I(x, t)|^2) \, dx,\end{aligned}\tag{2.22}$$

where $\mathcal{M} = \min \{\mu, D_1, D_2, (1 - \mathcal{R}_0)\}$ and $\mathcal{R}_0 < 1$. We can conclude that $\frac{dL_{\mathcal{E}_0}(t)}{dt} \leq 0$ if $\mathcal{R}_0 < 1$. From (Lemma 4.1. in [34]), one can determine

$$\lim_{t \rightarrow \infty} \int_{\Omega} [(S - S^0)^2 + (I - 0)^2 + |\nabla S|^2 + |\nabla I|^2] \, dx = 0.$$

Based on the above results and the following Poincaré inequality

$$\int_{\Omega} c_1 |S - \bar{S}|^2 \leq |\nabla S|^2 \, dx, \quad \int_{\Omega} c_2 |I - \bar{I}|^2 \leq |\nabla I|^2 \, dx,$$

we obtain

$$\lim_{t \rightarrow \infty} \int_{\Omega} [(S - \bar{S})^2 + (I - \bar{I})^2] \, dx = 0, \quad (2.23)$$

where $\bar{S} = \frac{1}{|\Omega|} \int_{\Omega} S(x, t) \, dx$ and $\bar{I} = \frac{1}{|\Omega|} \int_{\Omega} I(x, t) \, dx$. Hence,

$$\begin{aligned} |\Omega|(\bar{S}(t) - S^0)^2 &= \int_{\Omega} [\bar{S}(t) - S(x, t) + S(x, t) - S^0]^2 \, dx \\ &\leq \int_{\Omega} [\bar{S}(t) - S(x, t)]^2 \, dx + \int_{\Omega} [S(x, t) - S^0]^2 \, dx \\ |\Omega|(\bar{I}(t) - 0)^2 &= \int_{\Omega} [\bar{I}(t) - I(x, t) + I(x, t) - 0]^2 \, dx \\ &\leq \int_{\Omega} [\bar{I}(t) - I(x, t)]^2 \, dx + \int_{\Omega} [I(x, t) - 0]^2 \, dx. \end{aligned} \quad (2.24)$$

Therefore, one has $\bar{S}(t) \rightarrow S^0$ as $t \rightarrow \infty$ and $\bar{I}(t) \rightarrow 0$ as $t \rightarrow \infty$. All state variables are bounded based on Theorem 2.4. Then, for the functions $(F_1, F_2) \geq 0 \in C^2(\bar{\Omega})$ in the subsequence t_n , one can derive

$$\begin{aligned} \lim_{n \rightarrow \infty} \|S(\cdot, t_n) - F_1(\cdot)\|_{C^2(\bar{\Omega})} &= 0, \\ \lim_{n \rightarrow \infty} \|I(\cdot, t_n) - F_2(\cdot)\|_{C^2(\bar{\Omega})} &= 0, \end{aligned}$$

From the results in (2.23)-(2.24), then $F_1 \equiv S^0$ and $F_2 \equiv 0$. Therefore,

$$\lim_{n \rightarrow \infty} \|S(\cdot, t_n) - S^0\|_{C^2(\bar{\Omega})} = 0, \quad \lim_{n \rightarrow \infty} \|I(\cdot, t_n) - 0\|_{C^2(\bar{\Omega})} = 0.$$

□

Theorem 2.9 Let $\mathcal{R}_0 > 1$. Then, the globally asymptotical stability of equilibrium point \mathcal{E}_1 exists.

Proof The Lyapunov function is first given below

$$L_{\mathcal{E}_1}(t) = \int_{\Omega} \left[\frac{S^2(x, t)}{2} - S^* S(x, t) + \frac{I^2(x, t)}{2} - I^* I(x, t) \right] dx.$$

Differentiating it with respect to t and then one can provide

$$\frac{dL_{\mathcal{E}_1}(t)}{dt} = \int_{\Omega} \left[(S(x, t) - S^*) \frac{\partial S(x, t)}{\partial t} \right.$$

$$\begin{aligned} &\left. + (I(x, t) - I^*) \frac{\partial I(x, t)}{\partial t} \right] dx \\ &= \int_{\Omega} [(S(x, t) - S^*)(D_1 \Delta S(x, t) + \Lambda \\ &- \beta \delta S(x, t) I(x, t) - \mu S(x, t))] dx \\ &+ \int_{\Omega} [(I(x, t) - I^*)(D_2 \Delta I(x, t) + \beta \delta S(x, t) I(x, t) \\ &- (r + \epsilon + \mu + d) I(x, t))] dx. \end{aligned} \quad (2.25)$$

We see that the implementation of the divergence theorem together with the boundary conditions (2.4) and $\Lambda = \mu S^* + (r + \epsilon + \mu + d) I^*$ can give

$$\begin{aligned} \frac{dL_{\mathcal{E}_1}(t)}{dt} &\leq -\mu \int_{\Omega} (S - S^*)^2 \, dx \\ &- \int_{\Omega} \beta \delta S^* (I(x, t) - I^*)^2 \, dx - D_1 \int_{\Omega} |\nabla S(x, t)|^2 \, dx \\ &- D_2 \int_{\Omega} |\nabla I(x, t)|^2 \, dx \\ &\leq -\mathcal{P} \int_{\Omega} ((S(x, t) - S^*)^2 + (I(x, t) - I^*)^2 \\ &+ |\nabla S(x, t)|^2 + |\nabla I(x, t)|^2) \, dx, \end{aligned} \quad (2.26)$$

where $\mathcal{P} = \min \{\mu, \beta \delta S^*, D_1, D_2\}$. Hence, $\frac{dL_{\mathcal{E}_1}(t)}{dt} \leq 0$. From (Lemma 4.1. in [34]), one can obtain

$$\lim_{t \rightarrow \infty} \int_{\Omega} [(S - S^*)^2 + (I - I^*)^2 + |\nabla S|^2 + |\nabla I|^2] \, dx = 0.$$

Based on the above results and the following Poincaré inequality

$$\int_{\Omega} r_1 |S - \bar{S}|^2 \leq |\nabla S|^2 \, dx, \quad \int_{\Omega} r_2 |I - \bar{I}|^2 \leq |\nabla I|^2 \, dx,$$

then one has

$$\lim_{t \rightarrow \infty} \int_{\Omega} (S - \bar{S})^2 \, dx = 0, \quad \lim_{t \rightarrow \infty} \int_{\Omega} (I - \bar{I})^2 \, dx = 0, \quad (2.27)$$

where $\bar{S} = \frac{1}{|\Omega|} \int_{\Omega} S(x, t) dx$ and $\bar{I} = \frac{1}{|\Omega|} \int_{\Omega} I(x, t) dx$. Hence,

$$\begin{aligned} |\Omega|(\bar{S}(t) - U^*)^2 &= \int_{\Omega} [\bar{S}(t) - S(x, t) + S(x, t) - S^*]^2 dx \\ &\leq \int_{\Omega} [\bar{S}(t) - S(x, t)]^2 dx + \int_{\Omega} [S(x, t) - S^*]^2 dx \\ |\Omega|(\bar{I}(t) - I^*)^2 &= \int_{\Omega} [\bar{I}(t) - I(x, t) + I(x, t) - I^*]^2 dx \\ &\leq \int_{\Omega} [\bar{I}(t) - I(x, t)]^2 dx + \int_{\Omega} [I(x, t) - I^*]^2 dx. \end{aligned} \quad (2.28)$$

Hence, $\bar{S}(t) \rightarrow S^*$ as $t \rightarrow \infty$ and $\bar{I}(t) \rightarrow I^*$ as $t \rightarrow \infty$. For the functions $(H_1, H_2) \geq 0 \in C^2(\bar{\Omega})$ in the subsequence t_n , one has

$$\begin{aligned} \lim_{n \rightarrow \infty} \|S(\cdot, t_n) - H_1(\cdot)\|_{C^2(\bar{\Omega})} &= 0, \\ \lim_{n \rightarrow \infty} \|I(\cdot, t_n) - H_2(\cdot)\|_{C^2(\bar{\Omega})} &= 0. \end{aligned}$$

From the results in (2.27)-(2.28), then $H_1 \equiv S^*$ and $H_2 \equiv I^*$. Therefore,

$$\begin{aligned} \lim_{n \rightarrow \infty} \|S(\cdot, t_n) - S^*\|_{C^2(\bar{\Omega})} &= 0, \\ \lim_{n \rightarrow \infty} \|I(\cdot, t_n) - I^*\|_{C^2(\bar{\Omega})} &= 0. \end{aligned}$$

Therefore,

$$\begin{aligned} \mathcal{A} &= \begin{pmatrix} a_3 & a_1 & 0 & \cdots & \cdots & \cdots & 0 \\ a_4 & a_3 & a_2 & \ddots & & & \vdots \\ 0 & a_4 & a_3 & a_2 & \ddots & & \vdots \\ \vdots & \ddots & \ddots & \ddots & \ddots & \ddots & \vdots \\ \vdots & & \ddots & \ddots & \ddots & \ddots & \vdots \\ \vdots & & & \ddots & a_4 & a_3 & a_2 \\ 0 & \cdots & \cdots & 0 & a_5 & a_3 \end{pmatrix}, \\ \mathcal{B} &= \begin{pmatrix} b_3 & b_1 & 0 & \cdots & \cdots & \cdots & 0 \\ b_4 & b_3 & b_2 & \ddots & & & \vdots \\ 0 & b_4 & b_3 & b_2 & \ddots & & \vdots \\ \vdots & \ddots & \ddots & \ddots & \ddots & \ddots & \vdots \\ \vdots & & \ddots & \ddots & \ddots & \ddots & \vdots \\ \vdots & & & \ddots & b_4 & b_3 & b_2 \\ 0 & \cdots & \cdots & 0 & b_5 & b_3 \end{pmatrix}, \\ \mathcal{C} &= \begin{pmatrix} c_3 & c_1 & 0 & \cdots & \cdots & \cdots & 0 \\ c_4 & c_3 & c_2 & \ddots & & & \vdots \\ 0 & c_4 & c_3 & c_2 & \ddots & & \vdots \\ \vdots & \ddots & \ddots & \ddots & \ddots & \ddots & \vdots \\ \vdots & & \ddots & \ddots & \ddots & \ddots & \vdots \\ \vdots & & & \ddots & c_4 & c_3 & c_2 \\ 0 & \cdots & \cdots & 0 & c_5 & c_3 \end{pmatrix}, \\ \mathcal{D} &= \begin{pmatrix} d_3 & d_1 & 0 & \cdots & \cdots & \cdots & 0 \\ d_4 & d_3 & d_2 & \ddots & & & \vdots \\ 0 & d_4 & d_3 & d_2 & \ddots & & \vdots \\ \vdots & \ddots & \ddots & \ddots & \ddots & \ddots & \vdots \\ \vdots & & \ddots & \ddots & \ddots & \ddots & \vdots \\ \vdots & & & \ddots & d_4 & d_3 & d_2 \\ 0 & \cdots & \cdots & 0 & d_5 & d_3 \end{pmatrix}, \end{aligned}$$

3 Numerical analysis

3.1 Positivity

The M -matrix theory was introduced in [35] to provide the positivity of numerical scheme for each state variable, where the positivity criteria has important role to describe the behavior in mathematical epidemiology.

Theorem 3.1 *The positivity of (2.1)–(2.3) exists for all the time period $k = 1, 2, 3, \dots$, i.e., $S^k > 0, I^k > 0, Q^k > 0$ and $R^k > 0$.*

Proof Let Eqs. ((2.1)–(2.3)) be defined as the forms

$$\mathcal{A}S^{k+1} = S^k, \quad \mathcal{B}I^{k+1} = I^k, \quad \mathcal{C}Q^{k+1} = Q^k, \quad \mathcal{D}R^{k+1} = R^k. \quad (3.1)$$

and the entries for each matrix

$$\begin{aligned}
a_1 = a_5 &= -2v_1, \quad a_2 = a_4 = -v_1, \\
a_3 &= 1 + 2v_1 + \beta\delta\Delta t I_j^m + \mu\Delta t, \\
b_1 = b_5 &= -2v_2, \quad b_2 = b_4 = -v_2, \quad b_3 = 1 + 2v_2 \\
&\quad - \beta\delta\Delta t S_j^m + (r + \epsilon + \mu + d)\Delta t, \\
c_1 = c_5 &= -2v_3, \quad c_2 = c_4 = -v_3, \\
c_3 &= 1 + 2v_3 + (\varphi + d + \mu)\Delta t, \\
d_1 = d_5 &= -2v_4, \quad d_2 = d_4 = -v_4, \quad d_3 = 1 + 2v_4 + \mu\Delta t.
\end{aligned}$$

for $v = \frac{\Delta t}{\Delta x^2}$. Moreover, the column matrices of S^k, I^k, Q^k and R^k are

$$\begin{aligned}
S^k &= S_j^m + \Delta t \Lambda, \\
I^k &= I_j^m, \\
Q^k &= Q_j^m + \Delta t \epsilon I_j^m, \\
R^k &= R_j^m + \Delta t r I_j^m + \Delta t \varphi Q_j^m.
\end{aligned}$$

According to the role of M -matrix, one can derive

$$\begin{aligned}
S^{k+1} &= \mathcal{A}^{-1} S^k, \quad I^{k+1} = \mathcal{B}^{-1} I^k, \quad Q^{k+1} \\
&= \mathcal{C}^{-1} Q^k, \quad R^{k+1} = \mathcal{D}^{-1} R^k.
\end{aligned} \tag{3.2}$$

Since S^k, I^k, Q^k and R^k are positive. Then, the positivity of $S^{k+1}, I^{k+1}, Q^{k+1}$ and R^{k+1} are also satisfied by the M -matrix criterion for all the time period $k = 1, 2, 3, \dots$. \square

3.2 Consistency

The consistency is provided to determine the closeness between differential equations and numerical schemes obtained from Taylor' series.

Theorem 3.2 Let $\mathcal{Z}g = f$ be the general form of our dynamical system and $\mathcal{Z}_{\Delta x, \Delta t} h = f$ be the general form of the finite difference scheme. Then, the consistency can be achieved if the following condition is satisfied

$$\mathcal{Z}_{\Delta x, \Delta t} \theta - \mathcal{Z} \theta \rightarrow 0 \text{ as } (\Delta x, \Delta t) \rightarrow 0,$$

where $\theta(x, t)$ is any smooth function.

Proof We first define the following operator \mathcal{Z}

$$\mathcal{Z}\theta(x, t) = \left(\frac{\partial}{\partial t} - D_i \frac{\partial^2}{\partial x^2} \right) \theta(x, t), \tag{3.3}$$

for $\theta(x, t) = (S(x, t), I(x, t), Q(x, t), R(x, t))$.

Hence,

$$\begin{aligned}
\mathcal{Z}_{\Delta x, \Delta t} \theta(x, t) &= \frac{\theta_j^{m+1} - \theta_j^m}{\Delta t} - D_i \frac{\theta_{j-1}^{m+1} - 2\theta_j^{m+1} + \theta_{j+1}^{m+1}}{\Delta x^2}, \\
\text{for } \theta(x, t) &= (S(x_r, t_n), I(x_r, t_n), Q(x_r, t_n), R(x_r, t_n)).
\end{aligned} \tag{3.4}$$

By applying the following Taylor series

$$\begin{aligned}
S_j^{m+1} &= S(x_r, t_n) + \frac{\Delta t}{1!} S_t(x_r, t_n) + \frac{(\Delta t)^2}{2!} S_{tt}(x_r, t_n) \\
&\quad + \frac{(\Delta t)^3}{3!} S_{ttt}(x_r, t_n) + \dots \\
S_{j-1}^{m+1} &= \left(S(x_r, t_n) + \frac{\Delta t}{1!} S_t(x_r, t_n) + \frac{(\Delta t)^2}{2!} S_{tt}(x_r, t_n) \right. \\
&\quad \left. + \frac{(\Delta t)^3}{3!} S_{ttt}(x_r, t_n) + \dots \right) \\
&\quad - \frac{\Delta x}{1!} \left(S_x(x_r, t_n) + \frac{\Delta t}{1!} S_{xt}(x_r, t_n) + \frac{(\Delta t)^2}{2!} S_{xtt}(x_r, t_n) \right. \\
&\quad \left. + \frac{(\Delta t)^3}{3!} S_{xttt}(x_r, t_n) + \dots \right) \\
&\quad + \frac{(\Delta x)^2}{2!} \left(S_{xx}(x_r, t_n) + \frac{\Delta t}{1!} S_{xxt}(x_r, t_n) \right. \\
&\quad \left. + \frac{(\Delta t)^2}{2!} S_{xxtt}(x_r, t_n) + \frac{(\Delta t)^3}{3!} S_{xxttt}(x_r, t_n) + \dots \right) \\
&\quad - \dots \\
S_{j+1}^{m+1} &= \left(S(x_r, t_n) + \frac{\Delta t}{1!} S_t(x_r, t_n) + \frac{(\Delta t)^2}{2!} S_{tt}(x_r, t_n) \right. \\
&\quad \left. + \frac{(\Delta t)^3}{3!} S_{ttt}(x_r, t_n) + \dots \right) \\
&\quad + \frac{\Delta x}{1!} \left(S_x(x_r, t_n) + \frac{\Delta t}{1!} S_{xt}(x_r, t_n) + \frac{(\Delta t)^2}{2!} S_{xtt}(x_r, t_n) \right. \\
&\quad \left. + \frac{(\Delta t)^3}{3!} S_{xttt}(x_r, t_n) + \dots \right) \\
&\quad + \frac{(\Delta x)^2}{2!} \left(S_{xx}(x_r, t_n) + \frac{\Delta t}{1!} S_{xxt}(x_r, t_n) \right. \\
&\quad \left. + \frac{(\Delta t)^2}{2!} S_{xxtt}(x_r, t_n) + \frac{(\Delta t)^3}{3!} S_{xxttt}(x_r, t_n) + \dots \right) \\
&\quad + \dots
\end{aligned}$$

into

$$\begin{aligned}
&\frac{S_j^{m+1} - S_j^m}{\Delta t} - D_i \frac{S_{j-1}^{m+1} - 2S_j^{m+1} + S_{j+1}^{m+1}}{(\Delta x)^2} \\
&- \Lambda + \beta\delta S_j^{m+1} I_j^m - \mu S_j^{m+1} = 0,
\end{aligned}$$

and then employing the limit $(\Delta x, \Delta t) \rightarrow 0$ for the results, one can derive

$$\begin{aligned} \frac{S_j^{m+1} - S_j^m}{\Delta t} - D_1 \frac{S_{j-1}^{m+1} - 2S_j^{m+1} + S_{j+1}^{m+1}}{(\Delta x)^2} - \Lambda \\ + \beta \delta S_j^{m+1} I_j^m - \mu S_j^{m+1} \\ - \left(\frac{\partial S}{\partial t} - D_1 \frac{\partial^2 S}{\partial x^2} - \Lambda + (\beta \delta I + \mu) S \right) \rightarrow 0 \end{aligned} \quad (3.5)$$

as $(\Delta x, \Delta t) \rightarrow 0$.

Hence, the consistency is achieved by state variable S . Similarly, the consistency exists for the state variables I , Q and R . Therefore, for any smooth function $\theta(x, t)$, then $(\mathcal{Z}_{\Delta x, \Delta t} - \mathcal{Z})\theta(x, t) \rightarrow 0$ as $(\Delta x, \Delta t) \rightarrow 0$. \square

3.3 Simulations

In this subsection, we first provide the description of temporal model in Eq. (2.1) that is divided into 4 compartments. The susceptible individuals (S) indicate the healthy ones, i.e., the individuals are not infected by CoVid-19. The infected individuals (I) represent the individuals infected by CoVid-19 but the individuals do not develop symptoms (mild symptoms). The recovered individuals (R) are the individuals recovered from CoVid-19.

The susceptible (S) individual can be considered in an infection stage with the transmission rate (β) if there is a contact with an infected (I) individual ($S \rightarrow I$). The infected (I) individual can be tested for CoVid-19 with rate (η) and is then forced to quarantine ($I \rightarrow Q$). However, the infected (I) individual can recover from CoVid-19 with rate (r), i.e., it does not develop symptoms (mild symptoms) ($I \rightarrow R$). Moreover, the quarantined (Q) individual can recover from CoVid-19 after being isolated with rate φ ($Q \rightarrow R$). To provide the numerical results of spatio-temporal model in Eq. (2.2), we first present the following initial guess for each parameter and initial conditions for all state variables respectively

$$\begin{aligned} \Lambda = 0.07, \beta = 0.057, \delta = 0.4, \mu = 0.0019, \\ r = 0.057, \epsilon = 0.03, d = 0.001, \varphi = 0.7, \\ D_1 = 0.01, D_2 = 0.01, D_3 = 0.01, D_4 = 0.01, \\ S(x, 0) = 4, I(x, 0) = 3, Q(x, 0) = 0, R(x, 0) = 0. \end{aligned} \quad (3.6)$$

3.3.1 Numerical results of spatio-temporal model in Eq. (2.2)

According to initial guess of parameters and initial conditions of state variables in Eq. (3.6), we provide the simulations of susceptible (S), infected (I), quarantined (Q) and recov-

ered (R) individuals for disease-free ($\mathcal{R}_0 < 1$) and endemic ($\mathcal{R}_0 > 1$) equilibrium points. It follows from Eq. (2.8) for the basic reproduction number that the isolation rate (ϵ) is inversely proportional to the basic reproduction number (\mathcal{R}_0). The more isolation rate increases, the more basic reproduction number decreases. The number of susceptible individuals (S) to the disease-free equilibrium point (Fig. 2a) is greater when compared with the number of susceptible individuals (S) to the endemic equilibrium point (Fig. 2b) as the isolation rate increases (from $\epsilon = 0.03$ to $\epsilon = 0.9$). Moreover, as the isolation rate increases, the profile of infected individuals (I) goes to zero for the disease-free equilibrium point when compared with the profile of infected individuals (I) for the endemic equilibrium point as in Fig. 2c, d, where this also occurs in the profile of quarantined individuals. Thus, this indicates that increasing the isolation rate can effectively reduce the number of infected individuals. Moreover, the profile of recovered individuals for endemic equilibrium point is higher than the profile of recovered individuals for disease-free equilibrium point as in Fig. 3a, b. This is due to the profile of infected individuals decreasing to the disease-free equilibrium point. Figure 4a-d provide the profiles of susceptible, infected, quarantined and recovered individuals with the decreasing of social distancing rate (from $\delta = 0.4$ to $\delta = 0.04$). This is in line with Remark 1 when social distancing approaches to zero, this indicates the greater efforts for social distancing. At the disease-free equilibrium point, the increasing of isolation rate (from $\epsilon = 0.03$ to $\epsilon = 0.9$) is more effective than the decreasing of social distancing rate (from $\delta = 0.4$ to $\delta = 0.04$) in reducing the number of infected individuals. We can see these results based on the basic reproduction values, i.e., $\mathcal{R}_0 = 0.8751 < 1$ for change of isolation rate and $\mathcal{R}_0 = 0.9344 < 1$ for change of social distancing rate.

3.3.2 Fitting results of temporal model in Eq. (2.1)

The observed data of CoVid-19 in Fig. 5 consists of date and number of infected individuals (there is no effect of spatial). Then, this is the reason that the fitting results are only for temporal model in Eq. (2.1). As the first step, the total number of observed data of 750 data is divided into five parts ($D_1; D_2; D_3; D_4; D_5$) as in Fig. 5, where those five parts are defined as date ranges: $[D_1; D_2; D_3; D_4; D_5] = [09 \text{ Apr}-05 \text{ Sept } 2020; 06 \text{ Sept } 2020-01 \text{ Feb } 2021; 02 \text{ Feb}-01 \text{ Sept } 2021; 02 \text{ Sept}-29 \text{ Nov } 2021; 30 \text{ Nov } 2021-16 \text{ May } 2022]$ and each part has 150 data. The initial values of parameters ($\Lambda; \beta; \delta; \mu; r; \epsilon; d; \varphi$) in (3.6) are only as initial guess for computation, where it will change until the optimal values achieved (small difference between the model and observed data).

Because we only consider the temporal CoVid-19 model to conform to the observed data that only depends on time.

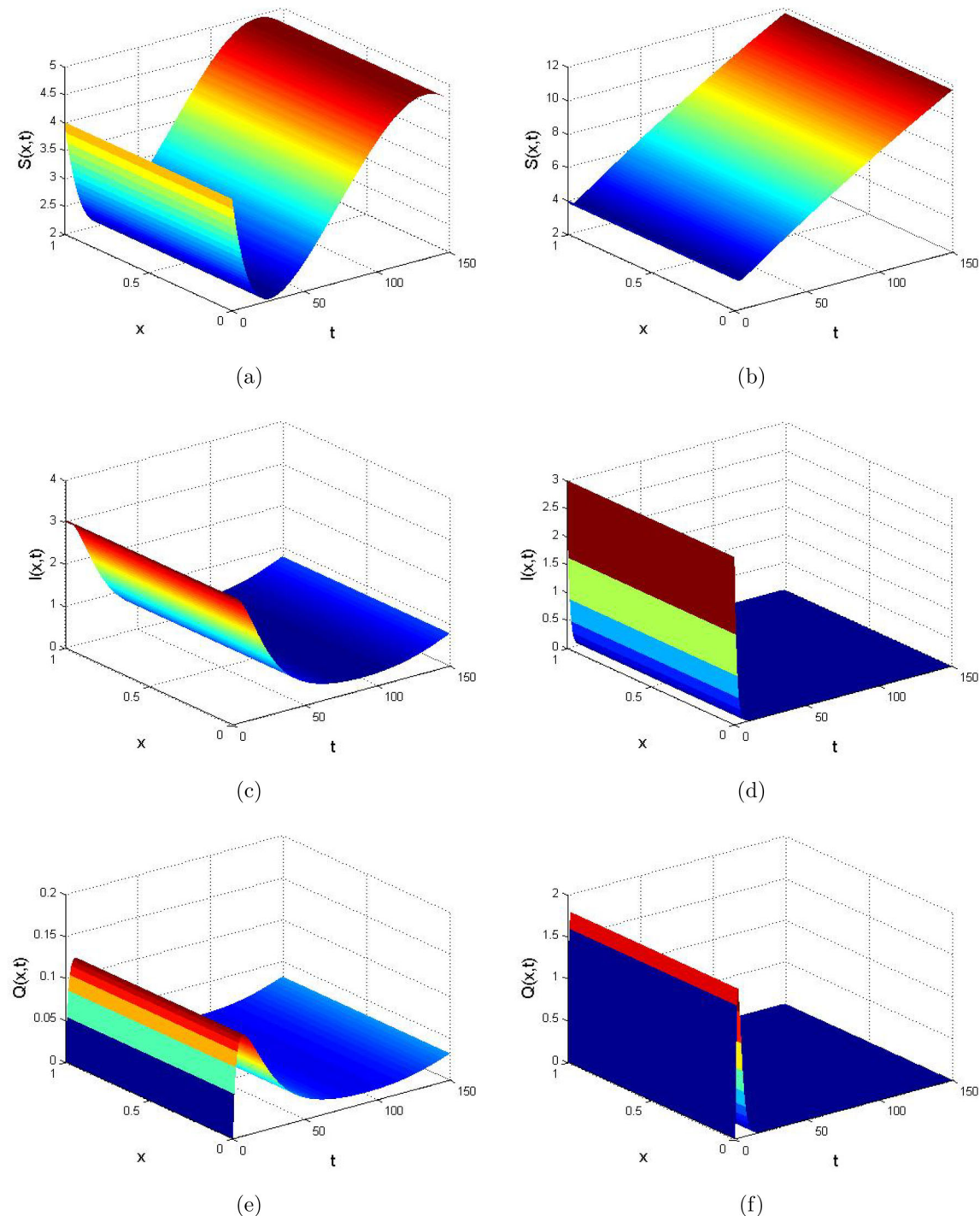


Fig. 2 The profiles of susceptible, infected and quarantined individuals of the spatio-temporal model for endemic equilibrium point ($\mathcal{R}_0 = 9.3437 > 1$) with social distancing ($\delta = 0.4$) and isolation

rate ($\epsilon = 0.03$) as in (b, c, e) and for disease-free equilibrium point ($\mathcal{R}_0 = 0.8751 < 1$) with social distancing ($\delta = 0.4$) and isolation rate ($\epsilon = 0.9$) as in (a, d, f)

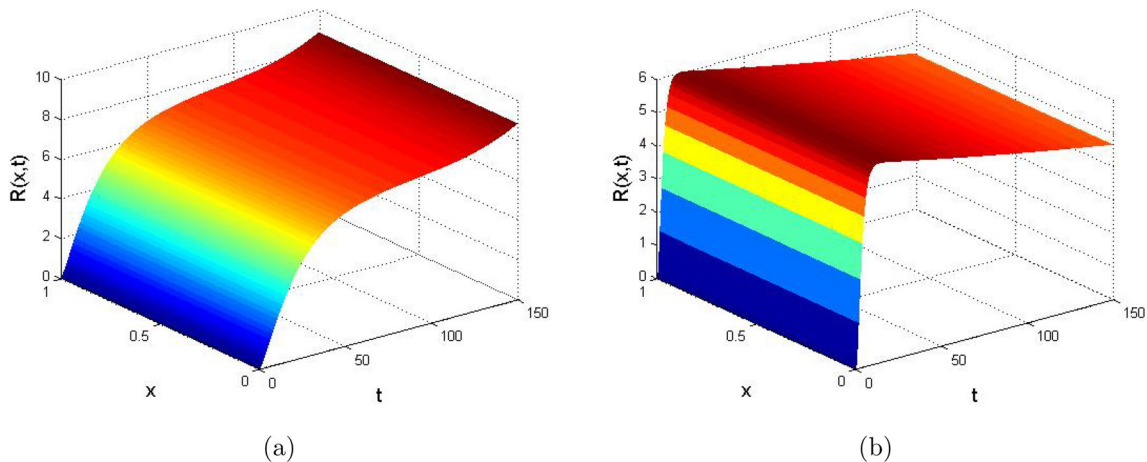


Fig. 3 **a** The profile of recovered individuals of the spatio-temporal model for endemic equilibrium point ($\mathcal{R}_0 = 9.3437 > 1$) with social distancing ($\delta = 0.4$) and isolation rate ($\epsilon = 0.03$) and **b** the profile

of recovered individuals of the spatio-temporal model for disease-free equilibrium point ($\mathcal{R}_0 = 0.8751 < 1$) with social distancing ($\delta = 0.4$) and isolation rate ($\epsilon = 0.9$)

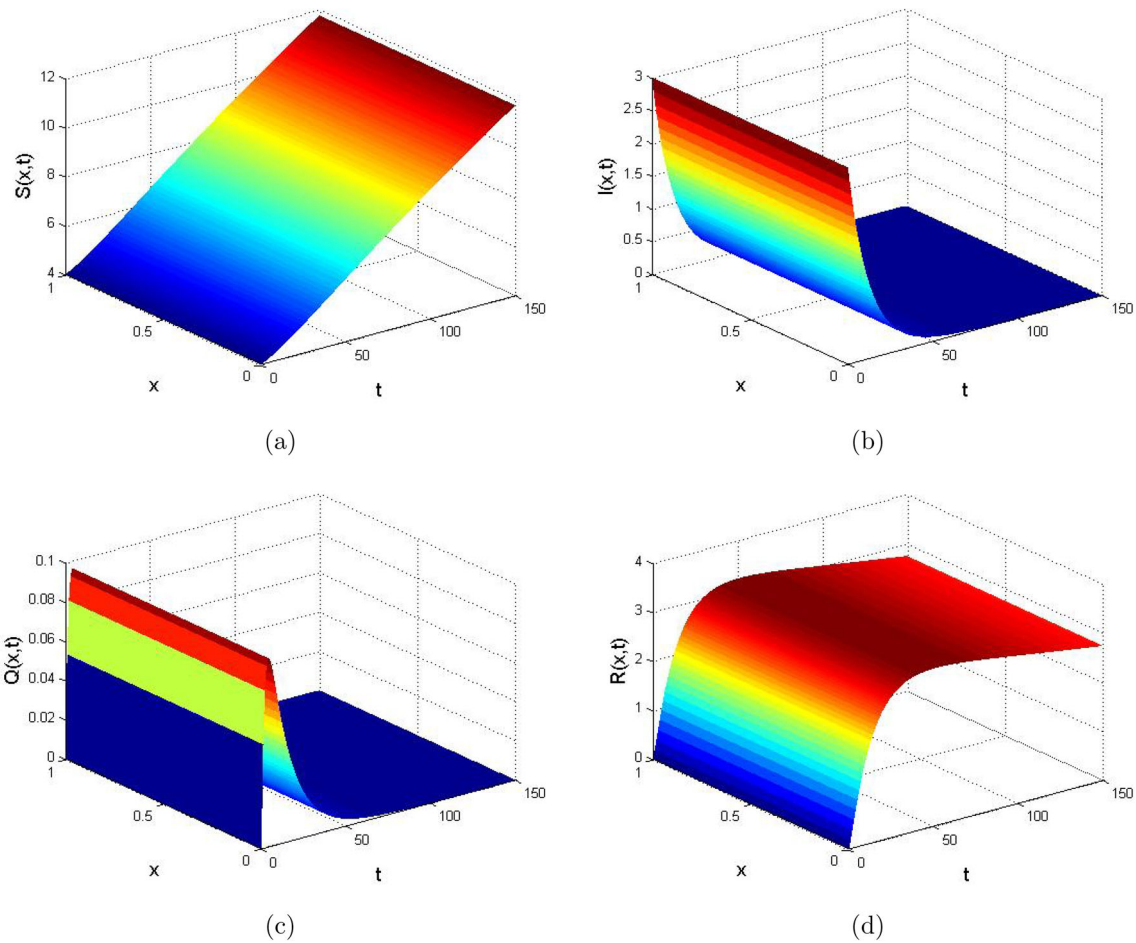


Fig. 4 The profiles of susceptible, infected, quarantined and recovered individuals of the spatio-temporal model for disease-free equilibrium point ($\mathcal{R}_0 = 0.9344 < 1$) with social distancing ($\delta = 0.04$) and isolation rate ($\epsilon = 0.03$) as in (a-d)

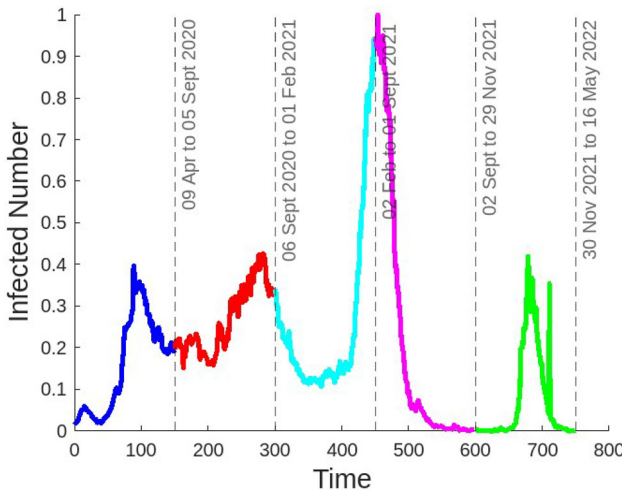


Fig. 5 Total infected number from 2020 Apr 09 till 2022 May 16. The total infected number is divided into five date ranges of \mathcal{D}_1 (blue color); \mathcal{D}_2 (red color); \mathcal{D}_3 (cyan color); \mathcal{D}_4 (magenta color); \mathcal{D}_5 (green color) = [09 Apr-05 Sept 2020; 06 Sept 2020–01 Feb 2021; 02 Feb-01 Sept 2021; 02 Sept-29 Nov 2021; 30 Nov 2021–16 May 2022]

Therefore, we first rewrite our temporal CoVid-19 model into the form

$$\mathcal{W}_t = \mathcal{M}(t, \mathcal{W}, \mathcal{N}), \quad (3.7)$$

where \mathcal{N} are the estimated parameters and \mathcal{W} consists of four state variables. Based on the numerical results of Eq. (3.7) using the fourth-order Runge–Kutta, then we determine the minimum values of \mathcal{N} between the predicted results and observed data through the $\text{RMSE}(\mathcal{N})$ with respect to Eq. (3.7).

The model-fitting results (green circle) with subject to Eq. (3.7) are provided in Fig. 12, where each part has its peaks. Moreover, the profiles of model parameters (obtained from the model-fitting with the observed data using least-square technique) are in Figs. 6, 7, 8, 9, 10 where each date range ($\mathcal{D}_1; \mathcal{D}_2; \mathcal{D}_3; \mathcal{D}_4; \mathcal{D}_5$) needs the different time to achieve the best estimates. It follows from the results, we can see that the date range \mathcal{D}_5 only needs 854 time (time required until the best fit) to reach the best fit estimated model parameters of $\Lambda, \beta, \delta, \mu, r, \epsilon, d, \varphi$. Hence, we can summarize the best fit estimation of parameters for each date range as follows

$$[\Lambda; \beta; \delta; \mu; r; \epsilon; d; \varphi]_{\mathcal{D}_1} = [0.0748; 0.0847; 1.1354; 0.0240; -0.0531; -0.1449; -0.0342; 19.4606],$$

$$[\Lambda; \beta; \delta; \mu; r; \epsilon; d; \varphi]_{\mathcal{D}_2} = [-0.0145; 0.0250; 2.7125; -0.0327; 0.2299; -0.1449; 0.0066; 6.4821],$$

$$[\Lambda; \beta; \delta; \mu; r; \epsilon; d; \varphi]_{\mathcal{D}_3} = [0.0761; 0.0348; 0.3089; 0.0017; 0.0276; 0.0227; -0.0026; 4.8535],$$

$$[\Lambda; \beta; \delta; \mu; r; \epsilon; d; \varphi]_{\mathcal{D}_4} = [-0.1750; 0.1968; 0.0849;$$

$$0.0051; 0.0351; -0.0545; 0.0024; 1.5934],$$

$$[\Lambda; \beta; \delta; \mu; r; \epsilon; d; \varphi]_{\mathcal{D}_5} = [-0.0040; 0.0809; 2.0982; -0.0145; 0.0783; 0.1237; -0.0004; 0.7294].$$

Moreover, the root mean square error (RMSE) values for each date range are given as follows: $[\mathcal{D}_1; \mathcal{D}_2; \mathcal{D}_3; \mathcal{D}_4; \mathcal{D}_5]_{\text{RMSE}} = [6.17\%; 9.64\%; 28.68\%; 8.77\%; 14.13\%]$. Based on those results, we can conclude that the date range of \mathcal{D}_1 is the best RMSE than four others and the date range of \mathcal{D}_3 is the worst RMSE than four others.

3.3.3 Fitting results of temporal model in Eq. (2.1) using neural network (NN)

It is similar with the previous sub section 3.3.2 which only considers the temporal CoVid-19 model in Eq. (2.1). Based on the results of estimated model parameters in the previous sub section, then the fitting results using neural network (blue line) are provided in Fig. 12. In this step, the Levenberg–Marquadt is as training function and Tangent Sigmoid and Purelin are as two activation functions shown in Fig. 11, where each hidden layer has 10 neurons (Fig. 12). Moreover, as in Fig. 13, each date range has an epoch value to reach the best validation performance, namely 667 epochs, 69 epochs, 1000 epochs, 71 epochs and 66 epochs respectively as in Table 1. It follows from the mean squared error of best validation performance, then the fitting results using neural network of temporal SIQR model are significant. The date range \mathcal{D}_3 has the smallest MSE and the date range \mathcal{D}_5 has the highest MSE. Then, there is no guarantee that a large number of epochs shall produce a smaller MSE (for example \mathcal{D}_1 and \mathcal{D}_2).

3.3.4 Fitting results of temporal model in Eq. (2.1) using extended Kalman filter (EKF)

In this subsection, we employ the same assumptions as in two previous subsections of least square technique and neural network that we consider the temporal CoVid-19 model. Therefore, the fitting of our CoVid-19 model are based on the dynamical system (2.1), where the workflow of EKF is generally represented in Fig. 14. In fact, the EKF consists of two main steps, including: predict step and update step, where $P(m|m)$ refers to the a priori estimate of covariance matrix and $C = \text{eye}(4)$ is the square matrix having 1s on the main diagonal, and 0s elsewhere. We first transform the dynamical system (2.1) into the form

$$Y(m+1) = Y(m) + F(Y(m)) + W(m),$$

where W and $F(Y(m))$ are the white noise and the righthand side of dynamical system (2.1) respectively and Y consists

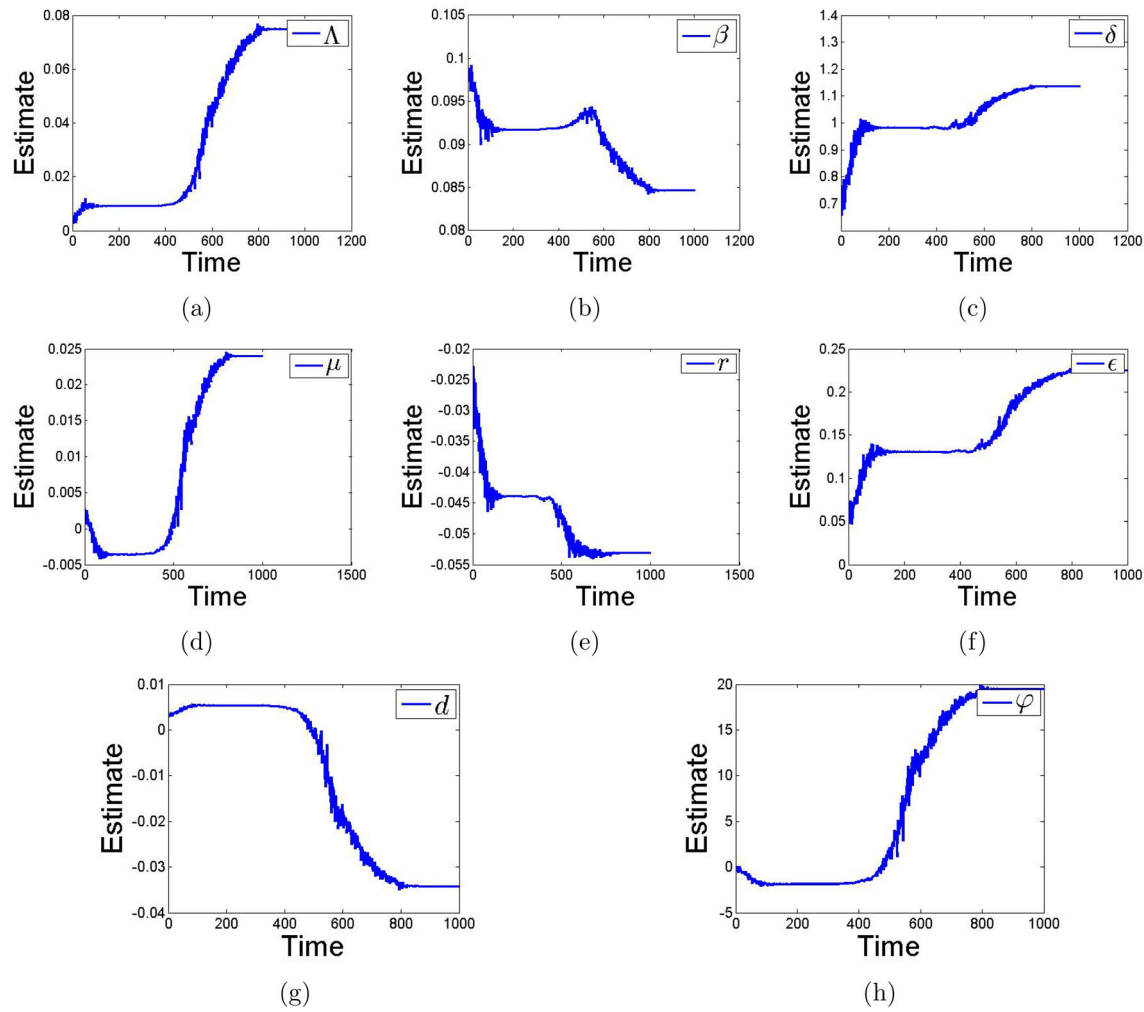


Fig. 6 SIQR model parameters for **(a)** birth rate, **b** transmission rate, **c** social distancing, **d** natural death rate, **e** cure rate related to infected, **f** isolation rate, **g** death rate related to disease, **h** cure rate related to isolation respectively in range of \mathcal{D}_1

of all state variables. By applying the forward difference over time, then one has

$$\begin{aligned} S^{m+1} &= S^m + \Delta t (\Lambda - \beta \delta S^m I^m - \mu S^m) + W_1^m, \\ I^{m+1} &= I^m + \Delta t \beta \delta S^m I^m - \Delta t (r + \epsilon + \mu + d) I^m + W_2^m, \\ Q^{m+1} &= Q^m + \Delta t \epsilon I^m - \Delta t (\varphi + d + \mu) Q^m + W_3^m, \\ R^{m+1} &= R^m + \Delta t r I^m + \Delta t \varphi Q^m - \Delta t \mu R^m + W_4^m. \end{aligned}$$

We suppose that \hat{Y} is the estimate of Y by using EKF. Then, the Jacobian matrix of $F(Y)$ at the estimate of \hat{Y} is given below

$$J(\hat{Y}) = \begin{pmatrix} \mathcal{M}_{11}(\hat{Y}) & \mathcal{M}_{12}(\hat{Y}) & \mathcal{M}_{13}(\hat{Y}) & \mathcal{M}_{14}(\hat{Y}) \\ \mathcal{M}_{21}(\hat{Y}) & \mathcal{M}_{22}(\hat{Y}) & \mathcal{M}_{23}(\hat{Y}) & \mathcal{M}_{24}(\hat{Y}) \\ \mathcal{M}_{31}(\hat{Y}) & \mathcal{M}_{32}(\hat{Y}) & \mathcal{M}_{33}(\hat{Y}) & \mathcal{M}_{34}(\hat{Y}) \\ \mathcal{M}_{41}(\hat{Y}) & \mathcal{M}_{42}(\hat{Y}) & \mathcal{M}_{43}(\hat{Y}) & \mathcal{M}_{44}(\hat{Y}) \end{pmatrix},$$

where

$$\begin{aligned} \mathcal{M}_{11} &= 1 + \Delta t (-\beta \delta \hat{I}^m - \mu), \quad \mathcal{M}_{12} = -\Delta t \beta \delta \hat{S}^m, \\ \mathcal{M}_{13} &= 0, \quad \mathcal{M}_{14} = 0, \\ \mathcal{M}_{21} &= \Delta t \beta \delta \hat{I}^m, \quad \mathcal{M}_{22} = 1 + \Delta t (\beta \delta \hat{S}^m \\ &\quad - (r + \epsilon + \mu + d)), \\ \mathcal{M}_{23} &= 0, \quad \mathcal{M}_{24} = 0, \\ \mathcal{M}_{31} &= 0, \quad \mathcal{M}_{32} = \Delta t \epsilon, \quad \mathcal{M}_{33} = 1 \\ &\quad + v_3 - \Delta t (\varphi + d + \mu), \quad \mathcal{M}_{34} = 0, \\ \mathcal{M}_{41} &= 0, \quad \mathcal{M}_{42} = \Delta t r, \\ \mathcal{M}_{43} &= \Delta t \varphi, \quad \mathcal{M}_{44} = 1 + v_4 - \Delta t \mu. \end{aligned}$$

Moreover, we choose the values of two tuning parameters: the covariance of process $Q = \text{diag}([10 \ 10 \ 10 \ 5])$ and the covariance of observation $R = \text{diag}([100 \ 10 \ 10 \ 1])$. The root mean square error (RMSE) and mean square error (MSE) are provided to ensure the accuracy of the model (Table 2).

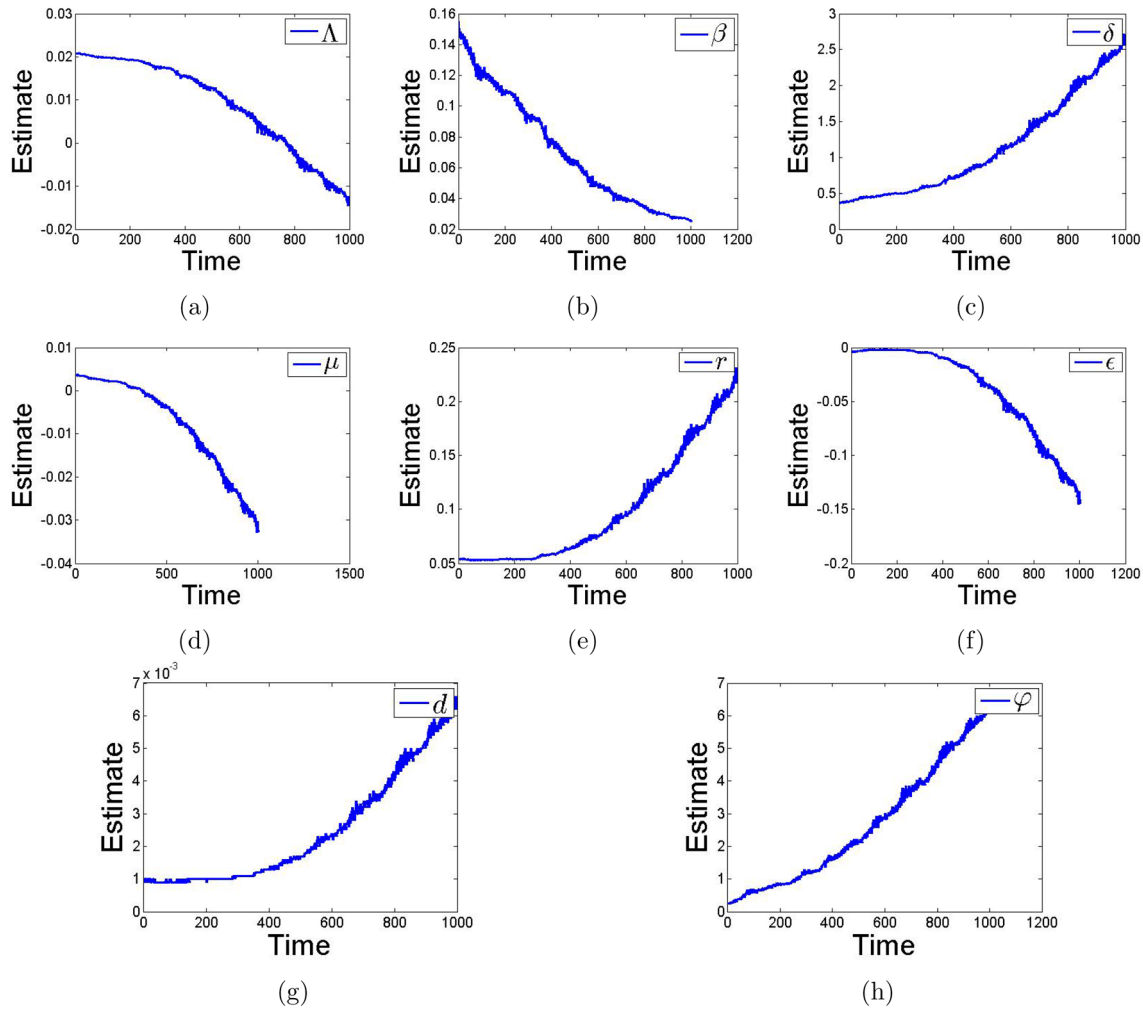


Fig. 7 SIQR model parameters for **(a)** birth rate, **b** transmission rate, **c** social distancing, **d** natural death rate, **e** cure rate related to infected, **f** isolation rate, **g** death rate related to disease, **h** cure rate related to isolation respectively in range of \mathcal{D}_2

The formula of those calculation methods can be stated below

$$\text{RMSE} = \sqrt{\frac{1}{N} \sum_{k=1}^N (\hat{Y}_k - Y_k)^2}, \quad \text{MSE} = \frac{1}{N} \sum_{k=1}^N (\hat{Y}_k - Y_k)^2.$$

Based on the fitting results of temporal SIQR model using EKF as in Fig. 15, we can conclude that the results are very significant for each five part of date range ($\mathcal{D}_1, \mathcal{D}_2, \mathcal{D}_3, \mathcal{D}_4, \mathcal{D}_5$). The Root Mean Square Error (RMSE), Mean Square Error (MSE) and Computation Time of EKF are shown in Table 3, where the smallest RMSE and MSE are achieved in the date range of \mathcal{D}_1 with the computation time 13.002942 in unit of seconds and the fastest computation of EKF is achieved in the date range of \mathcal{D}_5 with the RMSE 0.014 and the MSE 1.9550e–04. Moreover, the smallest RMSE and MSE of NN are shown in the date range of \mathcal{D}_1 with the computation time 11.442112 in unit of seconds and the fastest computation

of NN is provided in the date range of \mathcal{D}_2 with the RMSE 0.0253 and MSE 6.4100e–04 as in Table 2.

4 Conclusions

The spatio-temporal CoVid-19 model becomes our interest in this study. The positivity and boundedness are provided based on the standard positivity theorem. The Picard's iteration is employed to obtain the existence and uniqueness of solution for each state variable. Due to the presence of diffusion terms, we need the strategy of determining the Fourier expansion to provide the locally asymptotical stability for both equilibrium points. Moreover, the Lyapunov function is determined as the first step to prove the globally asymptotical stability for both equilibrium points. Based on the findings of numerical simulations, the increasing of isolation rate (from $\epsilon = 0.03$ to $\epsilon = 0.9$) is more effective than the decreasing of social

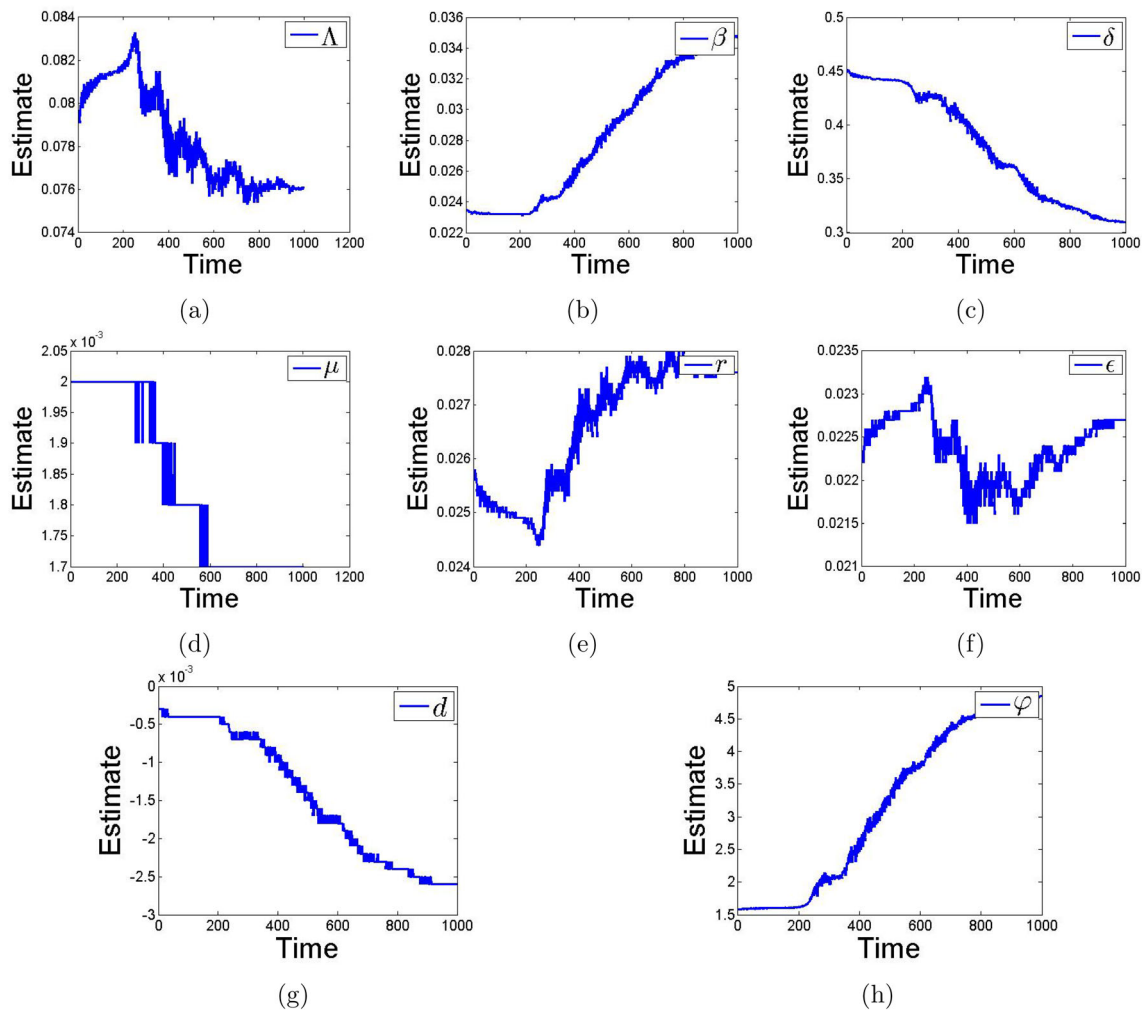


Fig. 8 SIQR model parameters for **(a)** birth rate, **b** transmission rate, **c** social distancing, **d** natural death rate, **e** cure rate related to infected, **f** isolation rate, **g** death rate related to disease, **h** cure rate related to isolation respectively in range of \mathcal{D}_3

distancing rate (from $\delta = 0.4$ to $\delta = 0.04$) in reducing the number of infected individuals, where these results are based on the basic reproduction values, i.e., $\mathcal{R}_0 = 0.8751 < 1$ for change of isolation rate and $\mathcal{R}_0 = 0.9344 < 1$ for change of social distancing rate.

The observed data of CoVid-19 consists of date and number of infected individuals (there is no effect of spatial). Then, this is the reason that the fitting results are only for temporal model in Eq. (2.1). The total number of observed data of 750 data is divided into five parts (\mathcal{D}_1 ; \mathcal{D}_2 ; \mathcal{D}_3 ; \mathcal{D}_4 ; \mathcal{D}_5), where those five parts are defined as date ranges: $[\mathcal{D}_1; \mathcal{D}_2; \mathcal{D}_3; \mathcal{D}_4; \mathcal{D}_5] = [09\text{ Apr-05 Sept 2020}; 06\text{ Sept 2020-01 Feb 2021}; 02\text{ Feb-01 Sept 2021}; 02\text{ Sept-29 Nov 2021}; 30\text{ Nov 2021-16 May 2022}]$ and each part has 150 data. Based on the estimated parameters for $\mathcal{W}_t = \mathcal{M}(t, \mathcal{W}, \mathcal{N})$, we provide the root mean square error (RMSE) values for each date range are given as follows: $[\mathcal{D}_1; \mathcal{D}_2; \mathcal{D}_3; \mathcal{D}_4; \mathcal{D}_5]_{\text{RMSE}} = [6.17\%; 9.64\%; 28.68\%; 8.77\%; 14.13\%]$, where the date range of

\mathcal{D}_1 is the best RMSE than four others and the date range of \mathcal{D}_3 is the worst RMSE than four others.

Based on the estimated parameters, then we employ the neural network to fit the temporal CoVid-19 model consisting of Levenberg–Marquadt as the training function and Tangent Sigmoid and Purelin as two activation functions. The fitting results using neural network of SIQR model are significant based on the mean squared error. Moreover, as in Fig. 13, each date range has an epoch value to reach the best validation performance, namely 667 epochs, 69 epochs, 1000 epochs, 71 epochs and 66 epochs respectively as in Table 1. It follows from the mean squared error of best validation performance, then the fitting results using neural network of temporal SIQR model are significant. The date range \mathcal{D}_3 has the smallest MSE and the date range \mathcal{D}_5 has the highest MSE. Then, there is no guarantee that a large number of epochs shall produce a smaller MSE (for example \mathcal{D}_1 and \mathcal{D}_2).

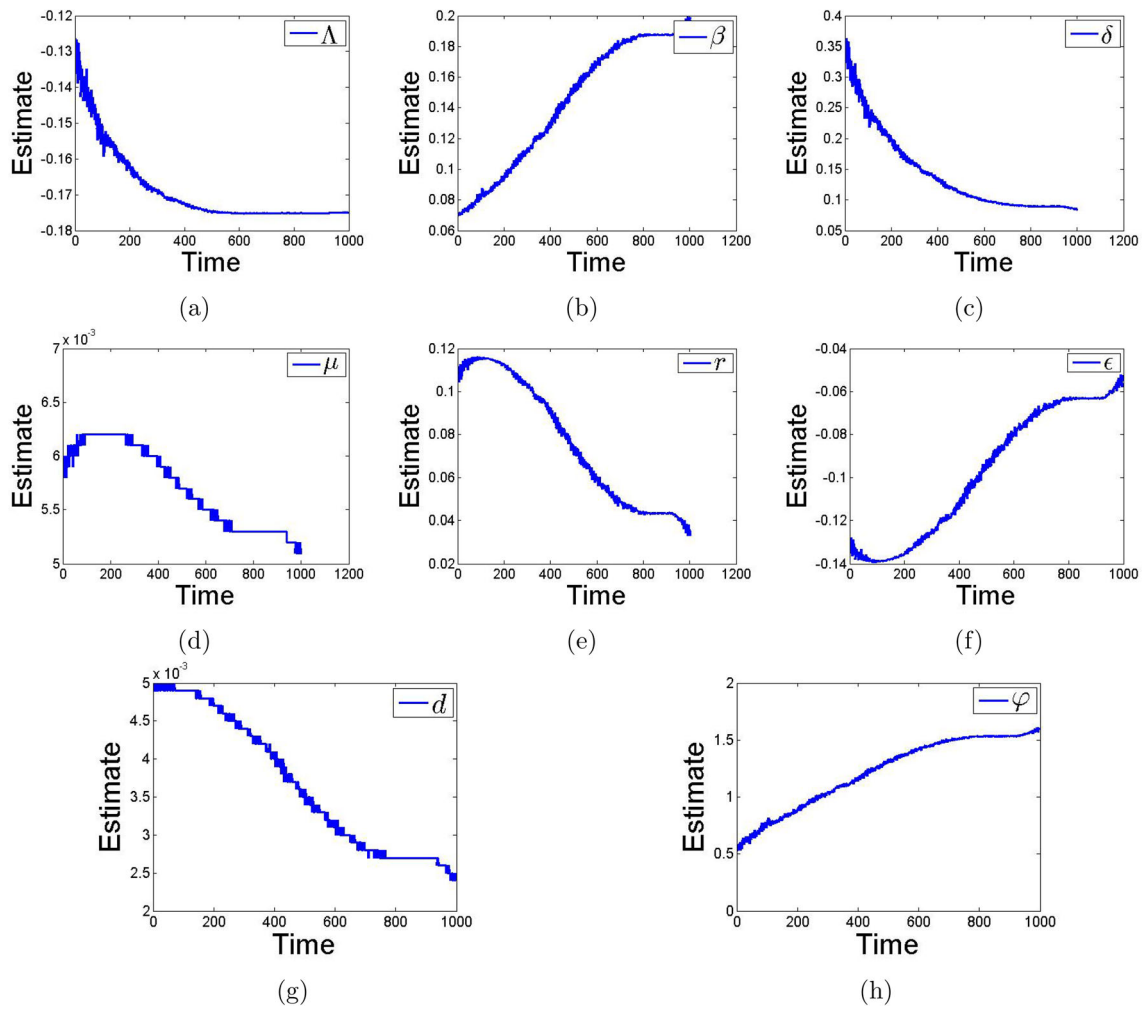


Fig. 9 SIQR model parameters for **a** birth rate, **b** transmission rate, **c** social distancing, **d** natural death rate, **e** cure rate related to infected, **f** isolation rate, **g** death rate related to disease, **h** cure rate related to isolation respectively in range of \mathcal{D}_4

Table 1 MSE of best validation performance and epoch using neural network (NN)

Accuracy	\mathcal{D}_1	\mathcal{D}_2	\mathcal{D}_3	\mathcal{D}_4	\mathcal{D}_5
MSE	7.0886e-10	5.9604e-10	6.5081e-11	2.7189e-09	3.271e-08
Epoch	667	69	1000	71	66

Table 2 Root Mean Square Error (RMSE), Mean Square Error (MSE) and Computation Time using neural network (NN)

Accuracy	\mathcal{D}_1	\mathcal{D}_2	\mathcal{D}_3	\mathcal{D}_4	\mathcal{D}_5
RMSE	0.0203	0.0253	0.0437	0.0241	0.0305
MSE	4.1044e-04	6.4100e-04	0.0019	5.8044e-04	9.2764e-04
Time (unit of seconds)	11.442112	5.920418	6.216077	7.314266	9.370994

Table 3 Root Mean Square Error (RMSE), Mean Square Error (MSE) and Computation Time using extended Kalman filter (EKF)

Accuracy	\mathcal{D}_1	\mathcal{D}_2	\mathcal{D}_3	\mathcal{D}_4	\mathcal{D}_5
RMSE	3.6542e-04	0.0013	0.0025	0.0044	0.014
MSE	1.3353e-07	1.8134e-06	6.3658e-06	1.9721e-05	1.9550e-04
Time (unit of seconds)	13.002942	13.028146	13.082653	12.979323	12.832805

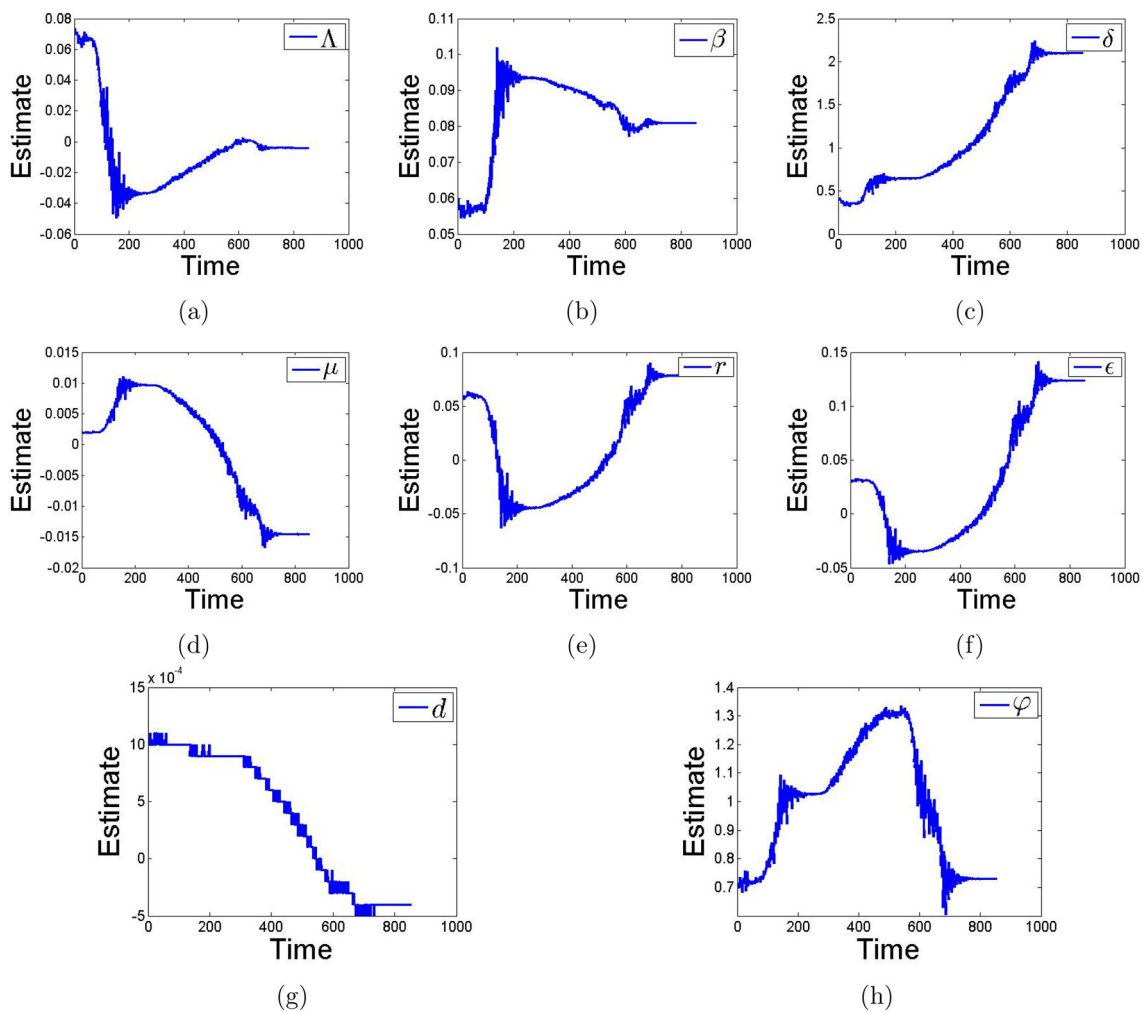


Fig. 10 SIQR model parameters for **(a)** birth rate, **b** transmission rate, **c** social distancing, **d** natural death rate, **e** cure rate related to infected, **f** isolation rate, **g** death rate related to disease, **h** cure rate related to isolation respectively in range of \mathcal{D}_5

Due to the significant results of fitting using extended Kalman filter, we also provide this technique by choosing $Q = \text{diag}([10 \ 10 \ 10 \ 5])$ and $R = \text{diag}([100 \ 10 \ 10 \ 1])$ for the covariance of process and observation respectively. Moreover, we have the smallest RMSE and MSE of EKF in the date range of \mathcal{D}_1 with the computation time 13.002942 s

and the fastest computation of EKF in the date range of \mathcal{D}_5 with the RMSE 0.014 and the MSE 1.9550e–04. The smallest RMSE and MSE of NN are shown in the date range of \mathcal{D}_1 with the computation time 11.442112 in unit of seconds and the fastest computation of NN is provided in the date range of \mathcal{D}_2 with the RMSE 0.0253 and MSE 6.4100e–04.

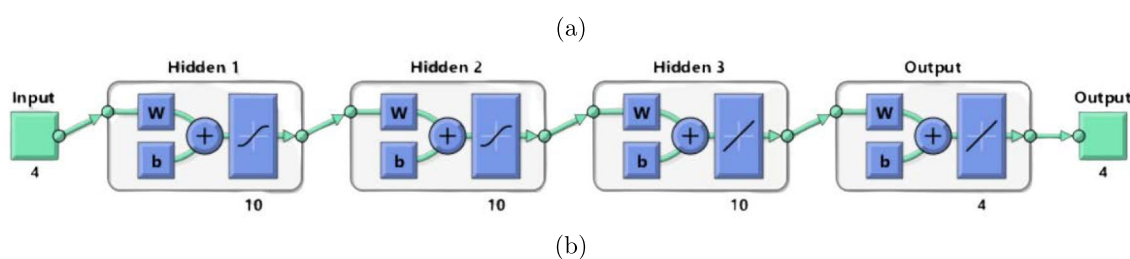
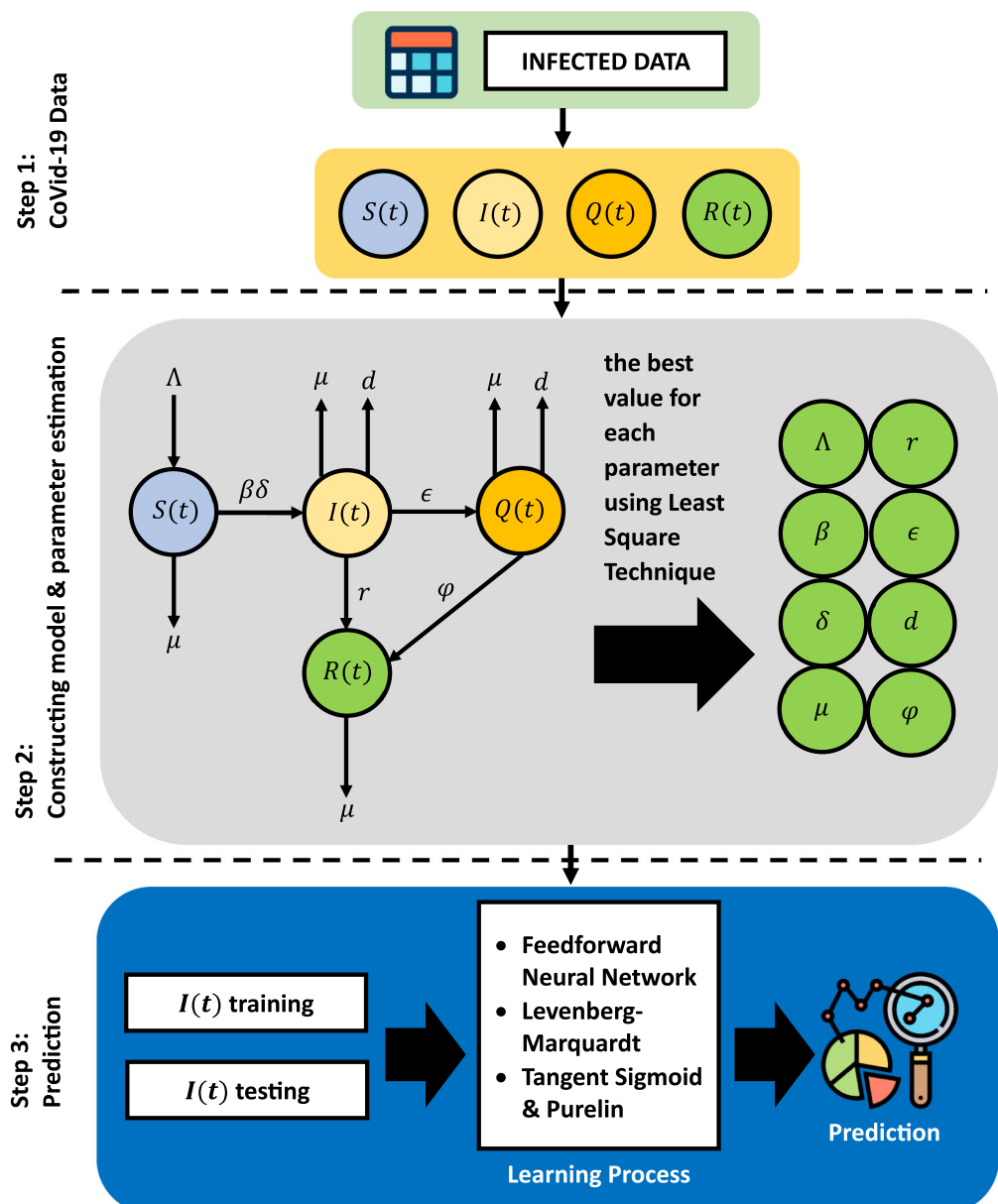


Fig. 11 **a** Workflow of SIQR predictive model, **b** architecture NN

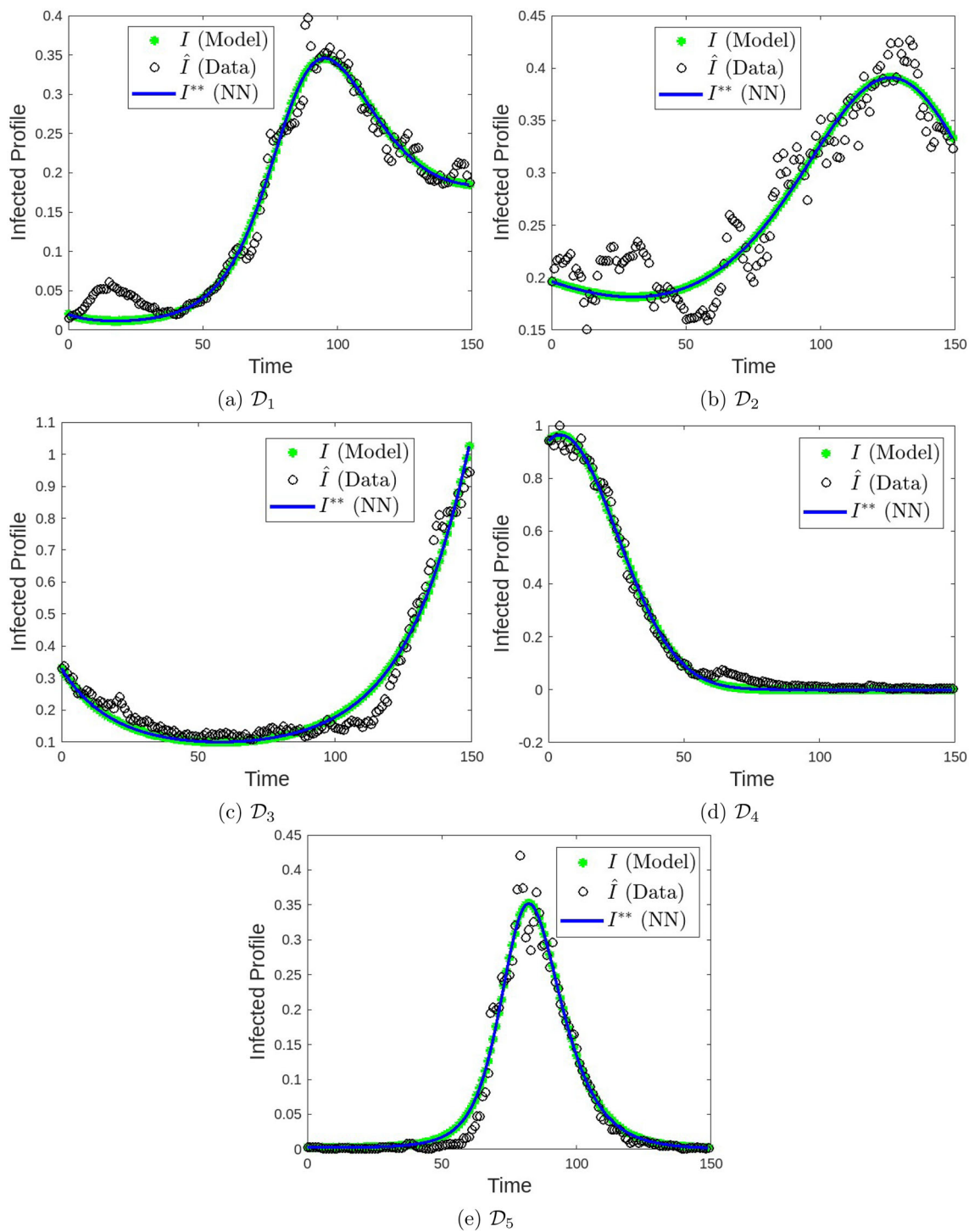


Fig. 12 Fitting results of temporal SIQR model in Semarang, Indonesia (I , \hat{I} , I^{**} refer to the model-fitting using least square technique, the observed data of infected number and the neural network respectively)

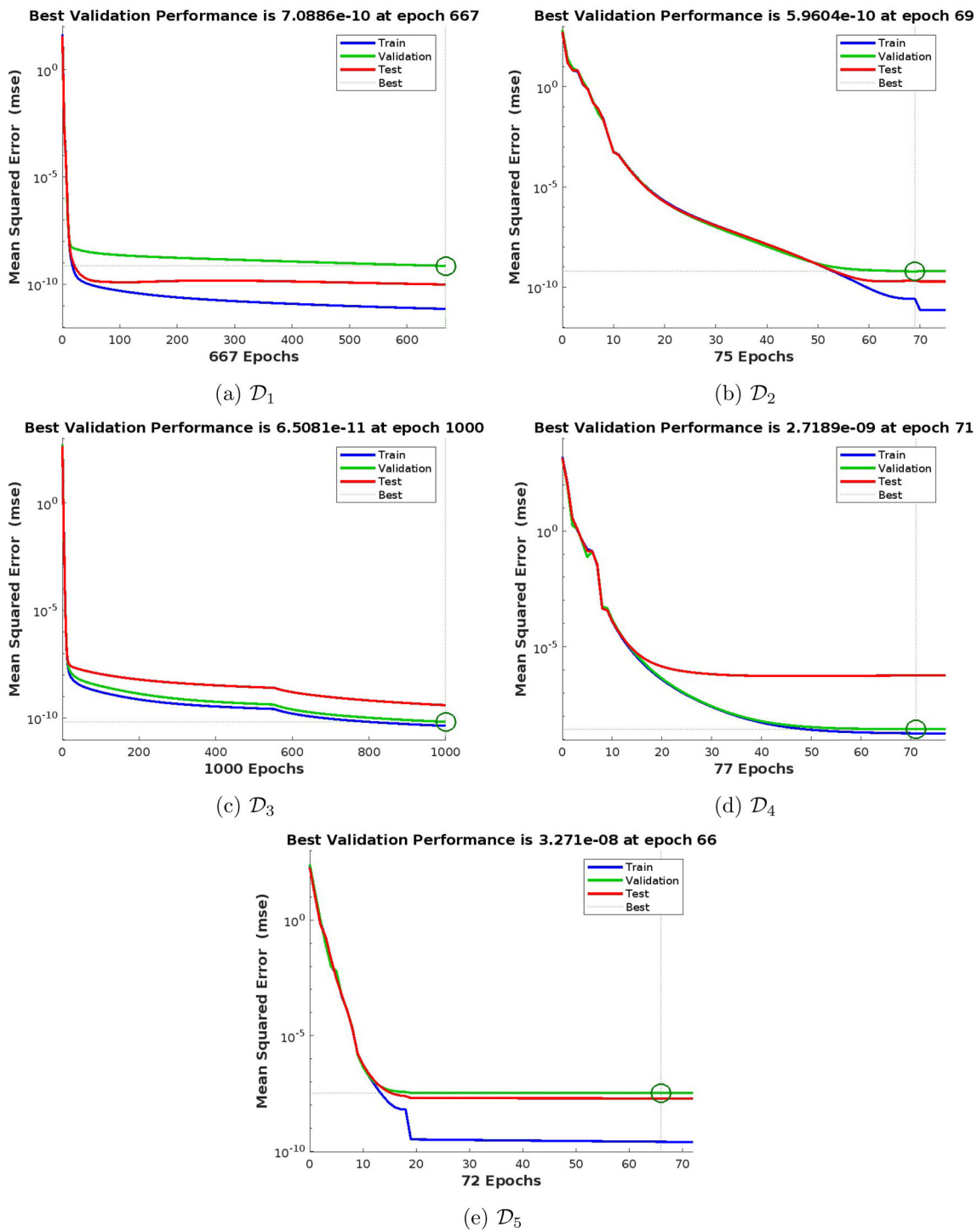


Fig. 13 Best validation performance using neural network of SIQR model in Semarang, Indonesia

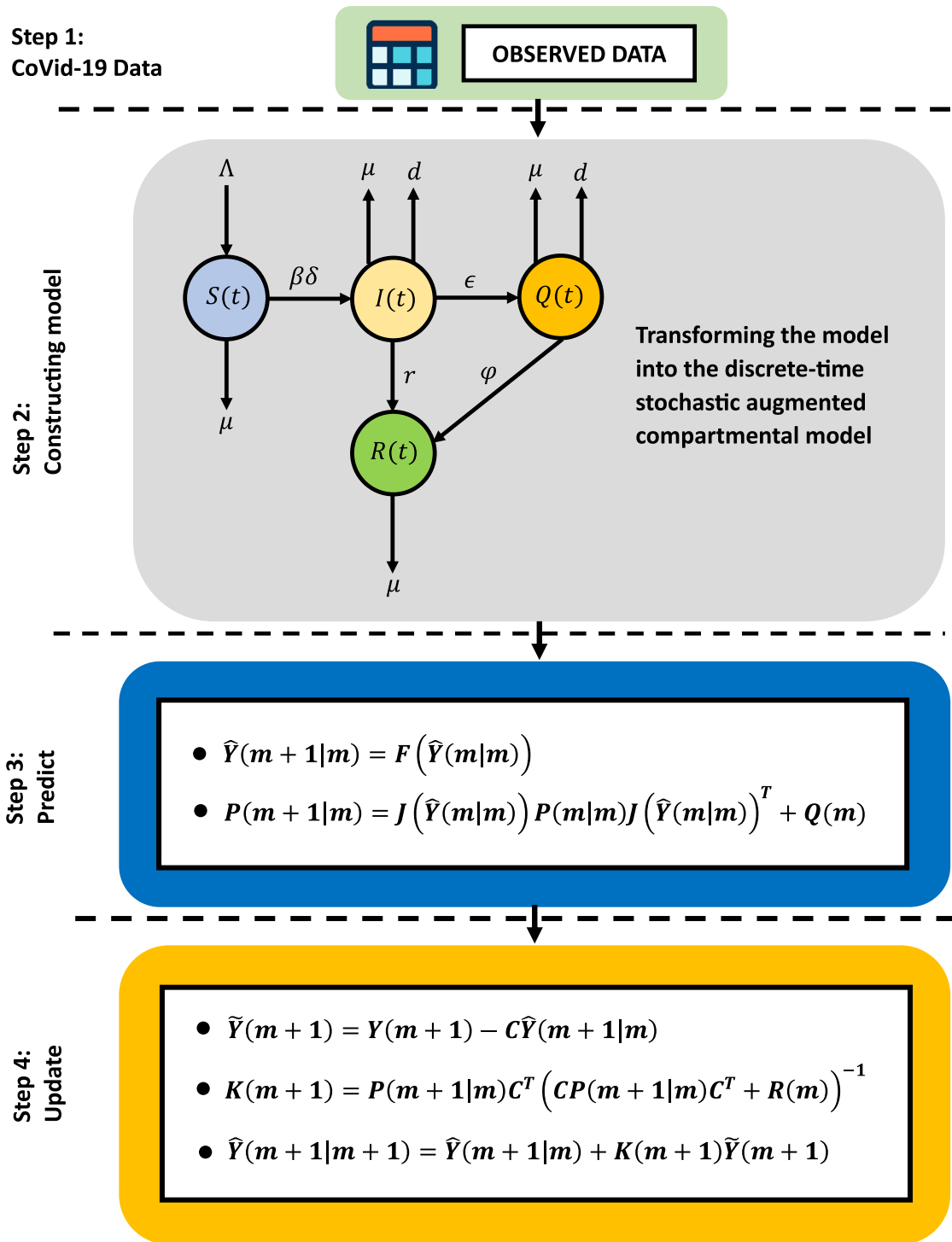


Fig. 14 Workflow of SIQR predictive model using extended Kalman filter (EKF)

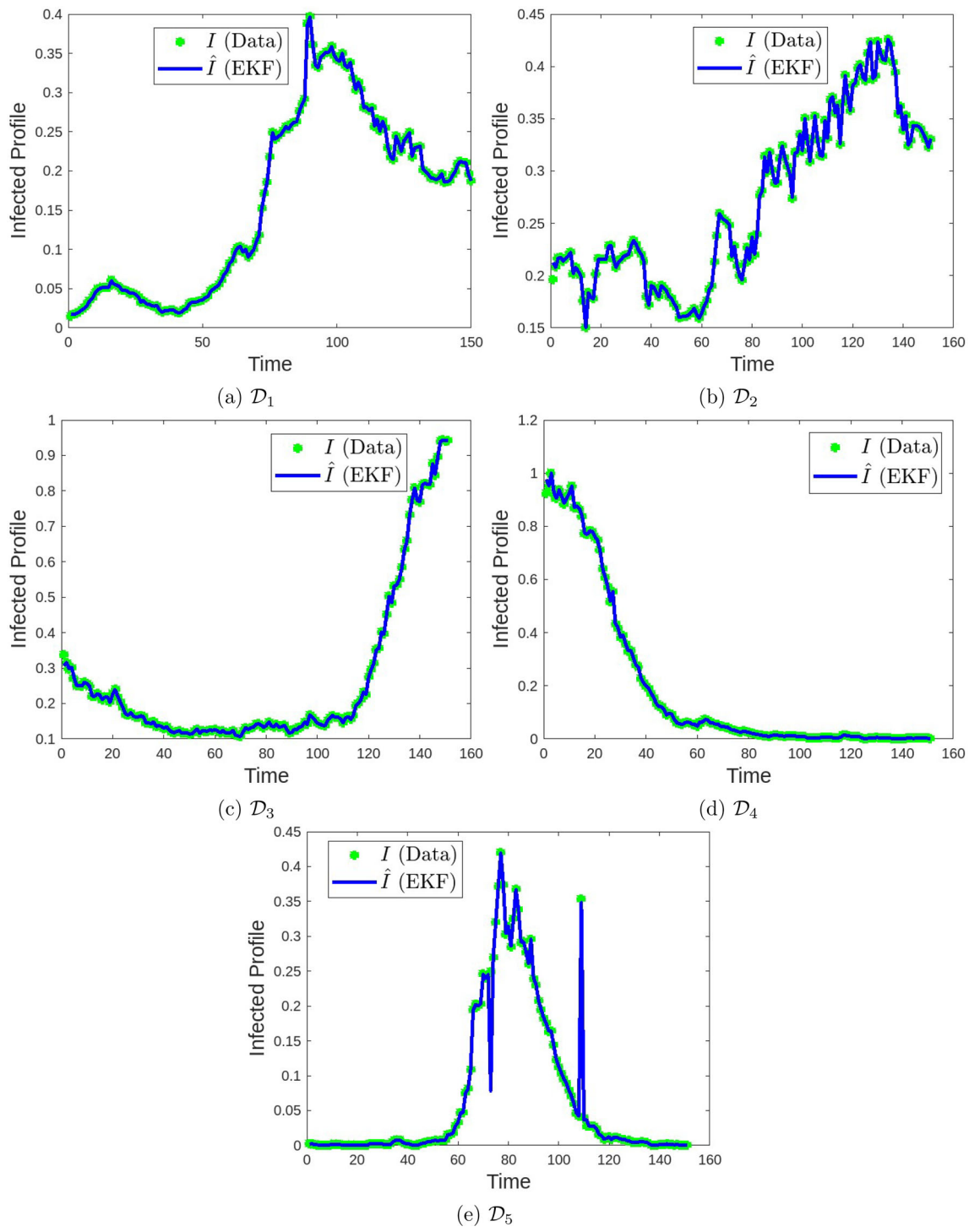


Fig. 15 Fitting results of temporal SIQR model using extended Kalman filter (EKF)

Source Code of Spatio-Temporal Model

```

clear all;clc;close all;
dt = 1;
dx = 0.05;
x = 0:dx:1;
t = 0:dt:149;
Nx = length(x);
Nt = length(t);
for i = 1:Nx
for j = 1:Nt
X(i,j) = x(i);
T(i,j) = t(j);
end
end
d1 = 0.01;
d2 = 0.01;
d3 = 0.01;
d4 = 0.01;
%% parameters
lambda=0.07;
beta=0.057;
delta=0.04; % or delta = 0.04
(disease-free)
mu=0.0019;
r=0.057;
epsilon=0.03; % or epsilon = 0.9
(disease-free)
d=0.001;
psi=0.7;
R0 = (lambda*beta*delta)/
(mu*(r+epsilon+mu+d))
lambda1 = d1*dt/(dx^2);
lambda2 = d2*dt/(dx^2);
lambda3 = d3*dt/(dx^2);
lambda4 = d4*dt/(dx^2);
%% initial condition
for i = 1:Nx
U(i,1)= 4;
end
for i = 1:Nx
V(i,1)= 3;
end
for i = 1:Nx
W(i,1)= 0;
end
for i = 1:Nx
Z(i,1)= 0;
end
%% main program implicit
for k = 1:Nt-1
% matrik A
for i = 1:Nx
for j = 1:Nx
if(i==j)
A(i,j) = 1 + 2*lambda1 + dt*mu
+ dt*delta*beta*V(i,k);
elseif(j-i==1 && i==1)
A(i,j) = -2*lambda1;
elseif(j-i==1 && i>1)
A(i,j) = -lambda1;
elseif(i-j==1 && i<Nx)
A(i,j) = -2*lambda1;
else
A(i,j) = 0;
end
end
end
% matrik B
for i = 1:Nx
for j = 1:Nx
if(i==j)
B(i,j) = 1 + 2*lambda2
- dt*delta*beta*U(i,k) + dt*(r+epsilon+mu+d);
elseif(j-i==1 && i==1)
B(i,j) = -2*lambda2;
elseif(j-i==1 && i>1)
B(i,j) = -lambda2;
elseif(i-j==1 && i<Nx)
B(i,j) = -lambda2;
elseif(i-j==1 && i==Nx)
B(i,j) = -2*lambda2;
else
B(i,j) = 0;
end
end
end
% matrik C
for i = 1:Nx
for j = 1:Nx
if(i==j)
C(i,j) = 1 + 2*lambda3
+ dt*(psi+d+mu);
elseif(j-i==1 && i==1)
C(i,j) = -2*lambda3;
elseif(j-i==1 && i>1)
C(i,j) = -lambda3;
elseif(i-j==1 && i<Nx)
C(i,j) = -lambda3;
elseif(i-j==1 && i==Nx)
C(i,j) = -2*lambda3;
else
C(i,j) = 0;
end
end
end
% matrik D
for i = 1:Nx
for j = 1:Nx
if(i==j)
D(i,j) = 1 + 2*lambda4 + dt*mu;
elseif(j-i==1 && i==1)
D(i,j) = -2*lambda4;
elseif(j-i==1 && i>1)
D(i,j) = -lambda4;
elseif(i-j==1 && i<Nx)
D(i,j) = -lambda4;
elseif(i-j==1 && i==Nx)
D(i,j) = -2*lambda4;
else
D(i,j) = 0;
end
end
end

```

```

D(i,j) = -2*lambda4;
else
D(i,j) = 0;
end
end
end
% boundary condition
for i = 1:Nx
BC_U(i,1) = U(i,k) + dt*lambda;
BC_V(i,1) = V(i,k);
BC_W(i,1) = W(i,k)
+ dt*epsilon*V(i,k);
BC_Z(i,1) = Z(i,k) + dt*r*V(i,k)
+ dt*psi*W(i,k);
end
U_new = inv(A)*BC_U;
V_new = inv(B)*BC_V;
W_new = inv(C)*BC_W;
Z_new = inv(D)*BC_Z;
for i = 1:Nx
U(i,k+1) = U_new(i,1);
V(i,k+1) = V_new(i,1);
W(i,k+1) = W_new(i,1);
Z(i,k+1) = Z_new(i,1);
end
end
figure(1)
g = surf(T,X,U);
ylabel('x','FontSize',14)
xlabel('t','FontSize',14)
zlabel('S(x,t)','FontSize',14)
%title('ENDEMIC EQUILIBRIUM',
'FontSize',14)
set(g,'LineStyle','none')
figure(2)
g = surf(T,X,V);
ylabel('x','FontSize',14)
xlabel('t','FontSize',14)
zlabel('I(x,t)','FontSize',14)
%title('ENDEMIC EQUILIBRIUM',
'FontSize',14)
set(g,'LineStyle','none')
figure(3)
g = surf(T,X,W);
ylabel('x','FontSize',14)
xlabel('t','FontSize',14)
zlabel('Q(x,t)','FontSize',14)
%title('ENDEMIC EQUILIBRIUM',
'FontSize',14)
set(g,'LineStyle','none')
figure(4)
g = surf(T,X,Z);
ylabel('x','FontSize',14)
xlabel('t','FontSize',14)
zlabel('R(x,t)','FontSize',14)
%title('ENDEMIC EQUILIBRIUM',
'FontSize',14)
set(g,'LineStyle','none')
% figure(5)
% plot(t,U,'b-','LineWidth',2.4)
% hold on
% plot(t,V,'g-','LineWidth',2.4)
% hold on
% plot(t,W,'r-','LineWidth',2.4)
% hold on
% plot(t,Z,'m-','LineWidth',2.4)
% ylabel('(S,I,Q,R)(t)', 'FontSize',14)
% xlabel('t','FontSize',14)
% %title('ENDEMIC EQUILIBRIUM',
% 'FontSize',14)

```

Acknowledgements There are no funders to report for this submission.

Author Contributions Mohammad Ghani: Formal analysis, Investigation, Methodology, Software, Writing—original draft, Writing—review and editing Ananta Adhi Wardana: Formal analysis, Investigation, Methodology, Software, Writing—original draft, Writing—review and editing Indah Fahmiyah: Conceptualization, Formal analysis, Investigation, Writing— original draft, Writing—review and editing Ratih Ardiati Ningrum: Conceptualization, Formal analysis, Investigation, Writing— original draft, Writing—review and editing.

Data availability The observed data of this study is provided at the link: <https://siagacorona.semarangkota.go.id/halaman/covid19pertahun/2020>.

Declarations

Conflict of interest The authors declare no conflict of interest in this paper.

Code availability All code was implemented in MATLAB. The source code was created by the authors themselves in this article.

References

1. Djalante R et al (2020) Review and analysis of current responses to COVID-19 in Indonesia: period of January to March 2020. *Prog Disaster Sci*. <https://doi.org/10.1016/j.pdisas.2020.100091>
2. Mahase E (2023) Covid-19: What do we know about XBB.1.5 and should we be worried? *BMJ* 380:153. <https://doi.org/10.1136/bmj.p153>
3. Demongeot J, Griette Q, Magal P (2020) SI epidemic model applied to COVID-19 data in mainland China. *R Soc Open Sci*. <https://doi.org/10.1098/rsos.201878>
4. Alenezi MN, Al-Anzi FS, Alabdulrazzaq H (2021) Building a sensible SIR estimation model for COVID-19 outspread in Kuwait. *Alex Eng J* 60(3):3161–3175. <https://doi.org/10.1016/j.aej.2021.01.025>
5. Alshammari FS, Khan MA (2021) Dynamic behaviors of a modified SIR model with nonlinear incidence and recovery rates. *Alex Eng J* 60(3):2997–3005. <https://doi.org/10.1016/j.aej.2021.01.023>
6. Ariffin MRK et al (2021) Mathematical epidemiologic and simulation modelling of first wave COVID-19 in Malaysia. *Sci Rep* 11(1):1–10. <https://doi.org/10.1038/s41598-021-99541-0>
7. Cooper I, Mondal A, Antonopoulos CG (2020) A SIR model assumption for the spread of COVID-19 in different communities. *Chaos Solitons Fractals* 139:110057. <https://doi.org/10.1016/j.chaos.2020.110057>
8. Kudryashov NA, Chmykhov MA, Vigdorowitsch M (2021) Analytical features of the SIR model and their applications to COVID-

19. Appl Math Model 90:466–473. <https://doi.org/10.1016/j.apm.2020.08.057>
9. ud Din R, Algehyne EA (2021) Mathematical analysis of COVID-19 by using SIR model with convex incidence rate. Results Phys 23(2020):1–6. <https://doi.org/10.1016/j.rinp.2021.103970>
10. Fernandez PM, Fernandez-Muniz Z, Cernea A, Luis Fernandez-Martinez J, Kloczkowski A (2023) Comparison of three mathematical models for COVID-19 prediction. Biophys J. <https://doi.org/10.1016/j.bpj.2022.11.1616>
11. Alqahtani RT (2021) Mathematical model of SIR epidemic system (COVID-19) with fractional derivative: stability and numerical analysis. Adv Differ Equ 1:2021. <https://doi.org/10.1186/s13662-020-03192-w>
12. Calafiore GC, Novara C, Possieri C (2020) A time-varying SIRD model for the COVID-19 contagion in Italy. Annu Rev Control 50(October):361–372. <https://doi.org/10.1016/j.arcontrol.2020.10.005>
13. Martínez V (2021) A modified SIRD model to study the evolution of the COVID-19 pandemic in Spain. Symmetry (Basel). <https://doi.org/10.3390/sym13040723>
14. Nanda MA et al (2022) The susceptible-infected-recovered-dead model for long-term identification of key epidemiological parameters of COVID-19 in Indonesia. Int J Electr Comput Eng 12(3):2900–2910. <https://doi.org/10.11591/ijecce.v12i3. pp2900-2910>
15. Cartocci A, Cevenini G, Barbini P (2021) A compartment modeling approach to reconstruct and analyze gender and age-grouped CoViD-19 Italian data for decision-making strategies. J Biomed Inform 118:103793. <https://doi.org/10.1016/j.jbi.2021.103793>
16. He S, Peng Y, Sun K (2020) SEIR modeling of the COVID-19 and its dynamics. Nonlinear Dyn 101(3):1667–1680. <https://doi.org/10.1007/s11071-020-05743-y>
17. Annas S, Isbar Pratama M, Rifandi M, Sanusi W, Side S (2020) Stability analysis and numerical simulation of SEIR model for pandemic COVID-19 spread in Indonesia. Chaos Solitons Fractals 139:110072. <https://doi.org/10.1016/j.chaos.2020.110072>
18. Marinov TT, Marinova RS (2022) Adaptive SIR model with vaccination: simultaneous identification of rates and functions illustrated with COVID-19. Sci Rep. <https://doi.org/10.1038/s41598-022-20276-7>
19. Sepulveda G, Arenas AJ, González-Parra G (2023) Mathematical modeling of COVID-19 dynamics under two vaccination doses and delay effects. Mathematics 11(2):1–30. <https://doi.org/10.3390/math11020369>
20. Parhusip HA, Trihandaru S, Wicaksono BAA, Indrajaya D, Sardjono Y, Vyas OP (2022) Susceptible vaccine infected removed (SVIR) model for COVID-19 cases in Indonesia. Sci Technol Indones 7(3):400–408. <https://doi.org/10.26554/sti.2022.7.3.400-408>
21. Fuady A, Nuraini N, Sukandar KK (2021) Targeted vaccine allocation could increase the COVID-19 vaccine benefits amidst its lack of availability: a mathematical modeling study in Indonesia. Vaccines (Basel) 9:462. <https://doi.org/10.3390/vaccines9050462>
22. Odagaki T (2020) Analysis of the outbreak of COVID-19 in Japan by SIQR model. Infect Dis Model 5(1982):691–698. <https://doi.org/10.1016/j.idm.2020.08.013>
23. Cao Z, Feng W, Wen X, Zu L, Cheng M (2019) Dynamics of a stochastic SIQR epidemic model with standard incidence. Phys A Stat Mech Appl 527:1–12. <https://doi.org/10.1016/j.physa.2019.121180>
24. Adnan et al (2022) Investigation of time-fractional SIQR Covid-19 mathematical model with fractal-fractional Mittage-Leffler kernel. Alex Eng J 61(10):7771–7779. <https://doi.org/10.1016/j.aej.2022.01.030>
25. Ahmed N, Raza A, Rafiq M, Ahmadian A, Batool N, Salahshour S (2021) Numerical and bifurcation analysis of SIQR model. Chaos Solitons Fractals 150:111133. <https://doi.org/10.1016/j.chaos.2021.111133>
26. Yangla J et al (2023) Fractional dynamics of a Chikungunya transmission model. Sci Afr. <https://doi.org/10.1016/j.sciac.2023.e01812>
27. Furati KM, Sarumi IO, Khalil AQM (2021) Fractional model for the spread of COVID-19 subject to government intervention and public perception. Appl Math Model 95:89–105. <https://doi.org/10.1016/j.apm.2021.02.006>
28. Ali Z, Rabiei F, Rashidi MM, Khodadadi T (2022) A fractional-order mathematical model for COVID-19 outbreak with the effect of symptomatic and asymptomatic transmissions. Eur Phys J Plus. <https://doi.org/10.1140/epjp/s13360-022-02603-z>
29. Arshad S, Khalid S, Javed S, Amin N, Nawaz F (2022) Modeling the impact of the vaccine on the COVID-19 epidemic transmission via fractional derivative. Eur Phys J Plus. <https://doi.org/10.1140/epjp/s13360-022-02988-x>
30. Das P, Nadim SS, Das S et al (2021) Dynamics of COVID-19 transmission with comorbidity: a data driven modelling based approach. Nonlinear Dyn 106:1197–1211. <https://doi.org/10.1007/s11071-021-06324-3>
31. Das P, Upadhyay RK, Misra AK et al (2021) Mathematical model of COVID-19 with comorbidity and controlling using non-pharmaceutical interventions and vaccination. Nonlinear Dyn 106:1213–1227. <https://doi.org/10.1007/s11071-021-06517-w>
32. Crokidakis N (2020) CoVid-19 spreading in Rio de Janeiro, Brazil: Do the policies of social isolation really work? Chaos Solitons Fractals 136:109930. <https://doi.org/10.1016/j.chaos.2020.109930>
33. Crokidakis N (2020) Modeling the early evolution of the CoVid-19 in Brazil; results from susceptible-infectious-quarantined-recovered (SIQR). Int J Mod Phys C 31:1–8. <https://doi.org/10.1142/S0129183120501351>
34. Lin Z, Pederson M (2004) Stability in a diffusive food-chain model with Michaelis–Menten functional response. Nonlinear Anal 57:421–433. <https://doi.org/10.1016/j.na.2004.02.022>
35. Fujimoto T, Ranade R (2004) Two characterizations of inverse positive matrices: the Hawkins–Simon condition and the Le Chatelierbraun principle. Electron J Linear Algebra ELA 11:59–65

Springer Nature or its licensor (e.g. a society or other partner) holds exclusive rights to this article under a publishing agreement with the author(s) or other rightsholder(s); author self-archiving of the accepted manuscript version of this article is solely governed by the terms of such publishing agreement and applicable law.